Grado en Ingeniería Electrónica Industrial

TRABAJO FIN DE GRADO

UNIVERSIDAD DE ALMERIA

ESCUELA SUPERIOR DE INGENIERÍA

"Modelization and optimization of a vacuum gripping-releasing device for micromanipulation"

Curso 2015/2016

Alumno/a:
Fabio Colombo

Directores:
Dr.D. Giovanni Legnani
Dr.D. Francisco Rodríguez Díaz

UNIVERSIDAD DE ALMERÍA
Escuela Superior de Ingeniería

UNIVERSITÀ DEGLI STUDI DI BRESCIA
Dipartimento di Ingegneria Meccanica Industriale
Corso di Laurea Magistrale in Ingegneria dell'Automazione Industriale

Trabajo Fin de Grado
Ingeniería Electrónica Industrial

MODELIZATION AND OPTIMIZATION OF A VACUUM GRIPPING-RELEASING DEVICE FOR MICROMANIPULATION

Modelado y optimización de una pinza de vacío de agarre y liberación para micromanipulación

Doble Título UNIBS-UAL
Mechatronics for Industrial Automation

Autor: FABIO COLOMBO

Director: Dr.D. Giovanni Legnani
Codirector. Dr D. Francisco Rodríguez Díaz

Almería (España), Julio 2016

Curso 2015-2016

Dubium sapientiae initium.

TABLE OF CONTENTS

INDEX OF FIGURES

RESUMEN

Este trabajo titulado *Modelado y optimización de una pinza de vacío de agarre y liberación para micromanipulación* consiste en un estudio preliminar sobre el modelado de elementos terminales para microrrobótica.

En el contexto de microrrobótica, a menudo es evidente que, durante la manipulación de objetos pequeño tamaño, la fase más crítica es el de la liberación. De hecho, las fuerzas microadesiçon (tales como las fuerzas electrostáticas o capilares) tienen más fuerza que el peso del objeto que está manipulando: es decir, la masa es tan pequeña que no se garantiza la liberación correcta por efecto único de la gravedad. En microrrobótica, como se muestra en la memoria de este Trabajo Fin de Grado, existen una serie de ténicas que se utilizan para agarrar y colocar pequeños objetos. Este trabajo se ha centrado en que el efector final actúe por succión. Estos sistemas Se componen de agujas finas y huecas, a través de las cuales se extrae una cierta cantidad de aire. Cuando esta aguja se acerca al objeto a ser manipulado, a través de aspiración, este se eleva. Por otra parte, se han analizado los dispositivos estudiados para integrar sus mecanismos internos de forma que se asegure la liberación de la pieza manipulada. Otros de los objetivos de este trabajo es analizar y modelar las dinámicas que carcaterizan el comportamienro de estas pinzas para que puedan ser mejoradas.

En la primera sección de la memora, se muestra una introducción general sobre microrrobótica y sus aspectos más importantes, particularmente se describirá el origen y la naturaleza de las fuerzas de microadesión. A continuación, se procederá a describir el sistema y las herramientas utilizadas, detallando el elemento terminal propuesto y sus principales característcias y prestaciones. Posteriormente se exponen los ensayos y pruebas experimentales llevadas a cabo, en los cuales se pretende destacar y cuantificar los aspectos esenciales del funcionamiento de la pinza. Estos esnayos representan el punto de partida para la construcción de modelos de dinámica de fluidos con el propósito de describir el funcionamiento de la pinza a fin de identificar los factores que deben ser optimizados (para mejorar la precisión y la repetibilidad).

1. AIM OF THE THESIS

Often in microrobotics, the most critical moment while manipulating very small components is the releasing phase: some adhesion forces, that can be stronger than gravitational force, makes this operation uncertain. As obvious, having an object that stays attached to the gripper during the releasing phase, it is a very unpleasant behaviour. We analysed those phenomena in the chapter 3. This work has the aim to model in order to optimize a vacuum gripper with a releasing mechanism by comprehending as much as possible the dynamics behind its functioning.

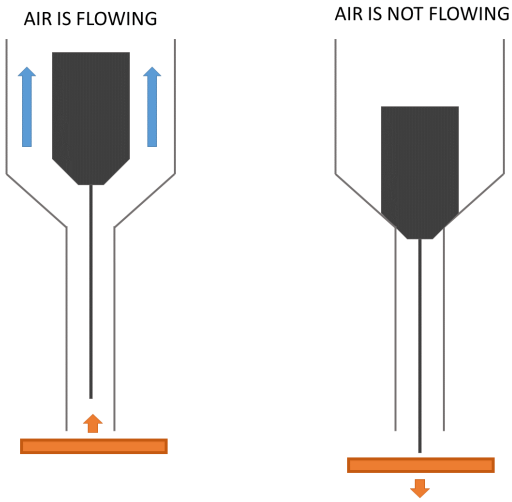

Figure 1 – Principle of functioning of the gripper studied.

The gripper studied in the course of this thesis, uses the vacuum as manipulation strategy, but tries to solve the issue of sticking forces adding a releasing mechanism. The pictures Figure 1, Figure 2, Figure 3 and Figure 4, allow to understand how this gripper works: it is composed by a holed needle that sucks the air from below; while doing this the component adhere to the tip blocking the passage of air and generating vacuum that retains the object. Inside the gripper, there is the so called *releasing mechanism* (Figure 4) that, at resting position, protrudes a little from the holed needle; as the air starts to pass, it is lifted of a few millimetres, freeing the tip and allowing the grasping. When the flow of air stops, it falls hitting the component and helping the releasing phase.

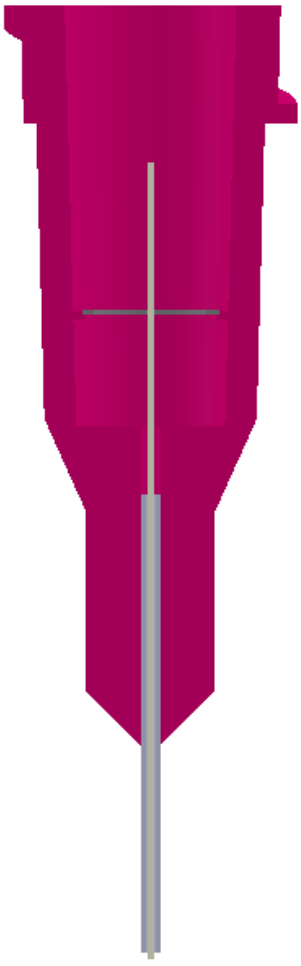

Figure 2 – Section of the assembled gripper

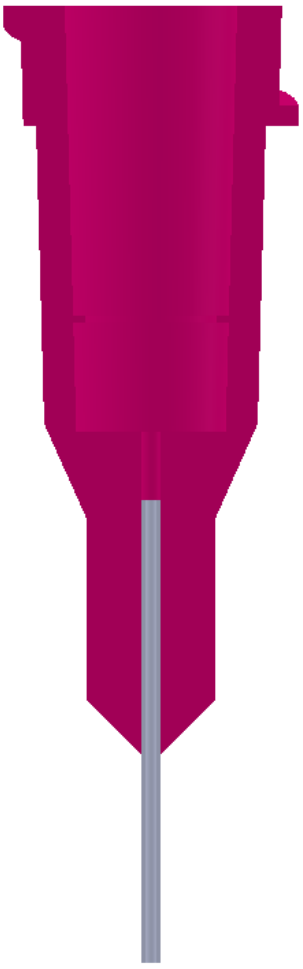

Figure 3 – Section without the releasing mechanism

Figure 4 – Releasing system

The gripper was invented by ITIA and UNIBS professors and researchers that nowadays obtained the patent for their end-effector [1]. As the Figure 4 clearly shows, they decided to add a small weight to their internal needle to increase the releasing chances.

Aim of this work was to modelize the behaviour of the gripper in order to optimise the releasing mechanism in all its components:

- Mass
- Geometry
- Operating pressures;
- Materials

During the development of this thesis we tried to vary some of those parameters to understand how this change modifies the functioning. The final objective is to guarantee the releasing in the 100% of cases.

2. MICROROBOTICS

The robotics is that branch of engineering that deals with those programmable mechatronics systems capable of sensing, computing and actuating in order to comply specific tasks. Those systems are generally referred to as *robots*. Those machines combine knowledge from different fields such as mechanics, electronics or controlling, but also many others more dependent to the task they are designed for (chemical, biological, optical…). The word robot descends from the ancient Slavic word *robota* that mean *hard work* and was often used referring to corvée work. Later on, the Czech writer Karel Čapek, in his play R.U.R. (1920), called robots the mindless and emotionless workers of the factory in which the drama takes place [2].

Nowadays robots are getting more and more common in our houses, as couriers and in thousands of other fields; however they are still mostly diffused in industrial applications guaranteeing efficiency. In particular manipulators, robots specifically designed to move, lift, place or assemble objects and components, are very common in factories with automated processes or in dangerous environments [3].

Figure 5 – Amazon robotic warehouse

Figure 6 – Amazon automated drone couriers

Since technologies evolves, industrial processes have to change too in order to be accurate enough to handle ever-smaller components. Microrobotics is the subset of robotics that studies robots with characteristic dimensions smaller than 1 mm. We would like to remark that the word *micro-robot* does not indicate a very small robot necessarily. Rather it connotes all whose robots with important and functional parts smaller than 1 mm. The robots in figures Figure 7 and Figure 8 are both considerable micro-robots: the first because it is a very small drone, the second because is capable of very small and movement beside it has also very small tools.

Reducing the size of robots has allowed to improve performance in many fields such as medicine and defence. For example in many hospitals surgeons can operate using the *Da Vinci System* which is one of the most advanced surgical robot: this system guarantees minimally invasive surgeries with evident benefits for the patient [4]. Another, closer to our experience, example is electronics: years after years robots allowed to assemble more powerful and much smaller CPUs, literally changing the everyday life.

Those micro-robots must be more advanced than their bigger counterparts and, moreover, are called to solve additional problems: while, in fact, the manipulators are twice smaller than normal, the components they must handle are thousands of times tinier. For this reason, actuators must guarantee higher precision and accuracy that can be achieved using, for example, deformable materials to lower the friction [5]. The side effects of those mechanisms are the nonlinear behaviour and the strong hysteresis, that makes them harder to model and raise the control costs. Then those actuators need more advanced sensors: while microscopes generally carry out the measurement of position, forces are not that easy to measure and nowadays those kind of transducers are very expensive or have a poor resolution [6].

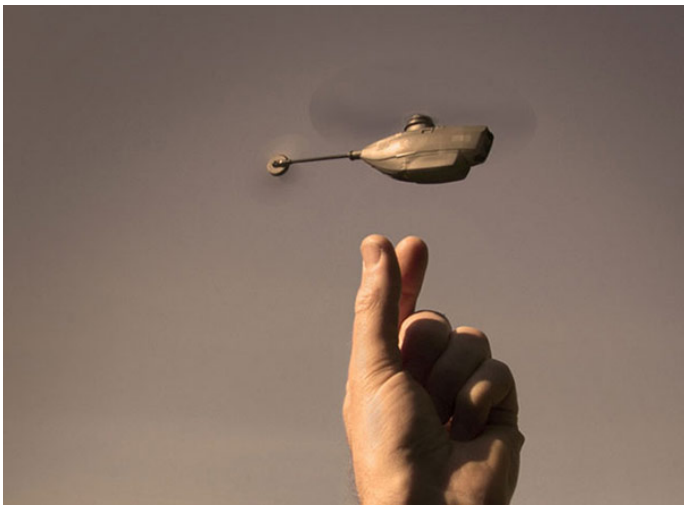

Figure 7 – Black Hornet Nano: is a micro unmanned aerial vehicle (UAV) used by British and Norwegian armies for recognition and surveillance

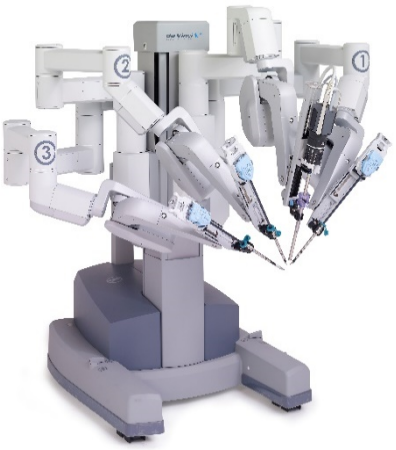

Figure 8 – Da Vinci Surgical System: surgical robot for minimally invasive operations

The supplementary difficulties are not only constructive or mechanical but involve also different control strategies and programming modalities. For example, very often in industrial realities, robots are programmed manually: the operator moves them remotely the first time and then the devices repeat the recorded trajectories. This method can't be used with micro-robots because human eye generally can't achieve the required precision due to the littleness of manipulated objects. Often downscaling the standard assembling strategies is not possible or very inefficient. Miniaturization of components or processes can be complex, because the physical phenomena involved, may not all change in the same manner as the scale is reduce. For instance, scaling down a violin generate a new instrument with a very different range of notes from the original one. The same happens for the majority of the application in microrobotics especially with all those phenomena not proportional to volume (like surface tension) [6].

Finally, the most significant problems in micro-world are micro-forces: moving objects of few microns is much different from handle bigger ones. In macroscopic applications, the focus of manipulating is on grabbing objects while the microrobotics must give a special importance in releasing too: as reasonable tiny components have tiny masses with consequent tiny gravitational force that many times is negligible compared to adhesion forces. These adhesive forces arise mostly, but not only, from surface tension, Van der Waals forces and electrostatic attraction.

While it is feasible to realize miniature version of the conventional robots' grippers, it seems not easy to win those sticking effects [7].

2.1. SENSING AND TRANSDUCING

As already touched on before, sensing is a critical issue in microrobotics: measure the position of objects being manipulated and/or the position of end-effectors, as well as the applied forces is never a trivial task [6].

2.1.1. POSITION

Visual methods are the most common solution to measure the position of micro-objects, since conventional methods cannot be used on such small components. Two tools are commonly exploited:

- Photonic or optical microscope;
- Scanning electron microscope.

Both allow to visualize micro-components of sizes between 1 μm and 1 mm, but both have some limitations. For example, the optical microscope lacks a good depth and width of field and robustness to illumination, which are problems that must be taken into account during the design of visual systems. The use of electron microscopy is an alternative method and has the advantage of an infinite depth of field but introduces a certain delay time (about 500 ms). This tool was initially developed to imaging micrometer-sized structures and not to carry out visual tasks. Nowadays the automatic measurement of the 3D position of micro-components remains a significant obstacle in automation of micromanipulation tasks: for example, every time that a vision system is set or moved, calibration is required. This particular task takes some time and must be iterate to improve performances.

2.1.2. FORCE

As in conventional robotic applications, also micromanipulation often requires the measurement and control of stress. The adjustment of force may be important to ensure a good grip during grasping (neither excessive nor insufficient), not risking to damage the manipulated components, or to calibrate the force of insertion during and assembly operation, or to detect contacts. The order of magnitude of the forces clearly depends on the application and, in general, varies from micro to millinewton. The measurement of the manipulation force applied is made difficult by absence of reliable measurement techniques for this level of force on robotic actuators. Indeed, the available technologies for multi-axis force sensors lack good resolutions.

2.2. ENVIRONMENTAL CONTROL

Since high precision and accuracy are critical requirements in micro-world, the environment where the robot operates must be controlled. Even minimum variations of temperature, humidity and, sometimes, chemical composition of air can compromise the reliability of an automatic micromanipulation process. Finally, environmental control means also to soften vibrations. In industrial realities micro-robots stay in closed chambers where hygrometric parameters are kept constant and the air filtered to avoid dust to enter [6].

2.3. MICRO-ACTUATORS

Micro-scales introduce specific fabrication limitations. The robots' components cannot be constructed by traditional fabrication processes that are replaced by unconventional (and much more expensive) ones: electrical discharge machining, electron-beam-inducted decomposition, laser sinterization, etc. Sometimes constructors build actuators and terminal tools together, in a single monolithic structure, in order to ease the assembling but with more fabrication problems, while other times, on the contrary, motors and links are physically two distinct objects (easier

fabrication but harder installation). Finally, the design of all this actuators requires a multidisciplinary knowledge in automation, microfabrication and material physics. Therefore, when possible, is normally preferable to use components with simpler design [6].

Actuators used in micro-scale may be a miniaturized version of conventional ones, but with finer construction parameters that make them more precise, or may be specifically designed: this means that there are no counterparts' versions in macro-world and often they exploits atypical physical principles. However, a common element of every actuator is the fact that there is a kind of conversion between energy of some sort into mechanical energy.

For example, piezoelectric materials are very common in those applications because are tiny, very fast and guarantee a good accuracy.

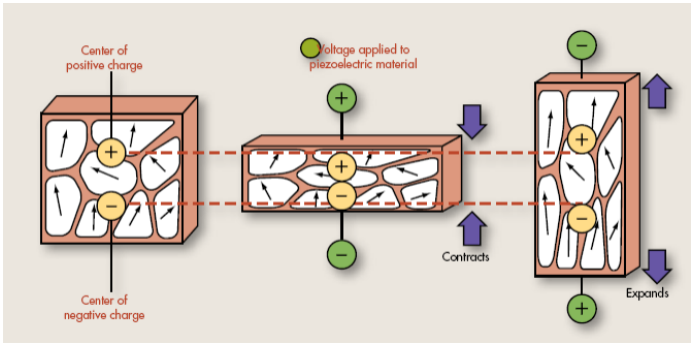

Figure 9 – Piezoelectric materials behaviour

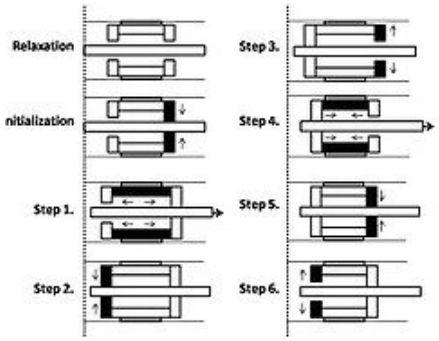

Figure 10 – Piezo-inchworm motor: steps required to move the internal part

As shown by the previous picture, piezoelectric materials stores in themselves positive and negative charges, that make the component stretch or shorten when a potential difference is applied. Both linear and rotary motors based on this technology exist. These piezoelectric motors use three groups of crystals: two of which are *Locking* and one *Motive*, permanently connected to either the motor's casing or stator (not both) and sandwiched between the other two, which provides the motion. These piezoelectric motors are fundamentally stepping motors, with each step comprising either two or three actions, based on the locking type. Another mechanism employs the use of surface acoustic waves (SAW) to generate linear or rotational motion. Electroactive polymers can achieve similar performances too, by with the advantage of an easier construction process [8].

A different solution, based on similar physical effects, consists in electrostatic motors that are based on the attraction and repulsion of electric charges, and can be somehow consider as the counterpart of conventional coil-based motors. The image Figure 11 shows an example of this kind of motor. The central rotor is the circular blue structure in the middle held to the substrate by the central bearing (structure in red). Around the perimeter of the rotor, are placed the stators (represented in blue too) with properly phased voltages. Those potential differences make the rotor turn. The material used to construct the actuator is polycrystalline silicon modelled with micromachining processes [9].

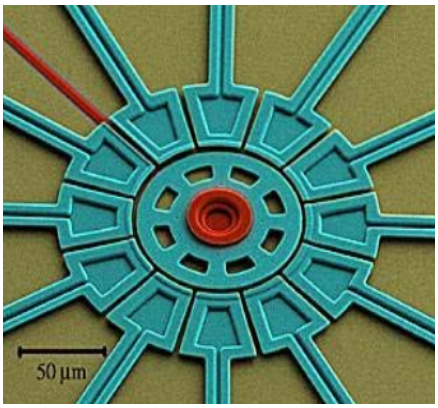

Figure 11 – Piezoelectric rotary motor

Micro-actuators exploits many effects of physics, not only related to electrical charges: shape memory alloys (SMA) represent an example. SMAs are materials able to “remember” their initial shapes: after being deformed, they can return to their initial configuration by being heated up. This behaviour is called super-elasticity [5].

2.4. MICROMANIPULATION STRATEGIES

As discussed before the manipulation strategies used in macro-world are not always replicable in micro-applications, but to gain a better comprehension of micro-objects is convenient to make some comparison: reasonably speaking, moving a grain of rice (2 mm) and a basketball ball (240 mm) require a different tool. The same proportion (about 1:100) covers the range of components

manipulated by micromanipulators. This should suggest that there are no standards and that every application must be studied separately.

In addition, in biomanipulation, another issue to overcome is biocompatibility. While materials such as silicon, silicon dioxide, as well as many polymers are biocompatible, the processes used to create the gripper can contaminate it. In this case, a coating with a biocompatible film can become necessary. As obvious, especially after those preconditions, in industrial reality are used many different strategies for manipulation but that can be generally classified as with or without contact [10].

2.4.1. MANIPULATION WITH CONTACT

The strategies based on this approach are many and based on several different physical principles but share some similarities:

- There is direct contact with moved objects;
- Can handle a wide range of shapes;
- Can exert forces.

The most common tools that work with contact are pliers or tweezers, which exists in thousands of different shapes, sizes, actuating principle and material depending on the use. Some of the actuating methods involve the use of electrostatics, pneumatics or shape memory alloys each one with their pros and cons. The cutting edge technology is moving the fingers using thermal biomorth actuators that exploits the mismatch of the thermal expansion coefficients between aluminium and silicon: while heating the structure bends closing the gripper [10].

As said in the paragraph 2.1.2, forces are not easy to be measured. But often, to keep under control the force applied on the fingers, the piezoresistive or capacitive properties of materials are exploited. Many conducing materials change their electrical resistance R with mechanical deformation (in some cases this change is remarkable). Moreover, for a given material, the so called gauge factor $g=(\Delta R/R)/(\Delta L/L)$ remains constant (where L is the length of the finger). Using those information it is possible to calculate the strain through the measurement of the variation of resistance: reversing the gauge factor formula can be found the deformation, and through the Young modulus the stress can be deduced. Typically the gouge factor is in the order unity for metals and much higher for semiconductors.

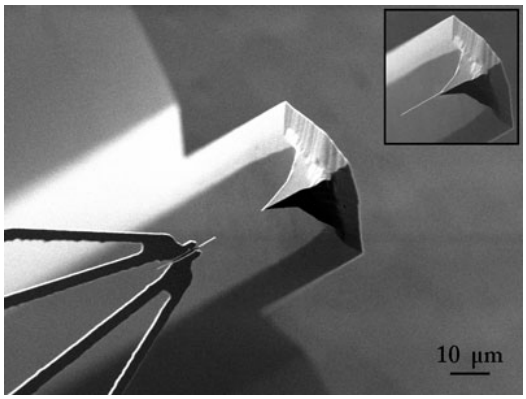

Figure 12 – Example of micro-gripper

The grippers based on friction can count on quite high accuracy but are influenced by the geometry of the object and can damage them through scratches or deformations and for this reason is required particular caution when contact is on functional parts. Moreover, each finger cause sticking effects and their relative movement is often asymmetrical and always need at least two surfaces of contact. As described before, the force that they can exert is strongly related to the actuation principle but it varies from µN to N [5].

Less conventional end-effectors use other principles such as electrostatics. It consists in establishing a potential difference between the gripper and the surface where the object is, inducting a charge on the object itself that therefore stays attracted to the robot. It works with both conductive and non-conductive materials. This method guarantees a comparable accuracy to friction grippers' but with less risk of damaging components (due mostly to inductive interference). The grip force is in the order of mN but depends on the charged surface's extension and retainable along the grip surface. Grip stiffness depends on the friction [7].

Since capillary forces assume high importance in microscale, many grippers exploits them. They are used due to their flexibility and reliability, because have a compliant behaviour, a self-centring effect and the capability of grasping small and light components in a wide range of materials and shapes. Another benefit given by those end-effectors is the "bumper" effect thanks to the film of fluid between the gripper and the objects. To release parts grasped by capillary grippers there are several ways:

- Scratching against an edge;
- Using two different fluids;

- Changing the gripper curvature;
- Electrowetting.

The side effects of the method are the traces left on the surfaces that must be removed (by evaporation) through a following heating and may be not ideal to use with microelectronic or hydrophobic components [7].

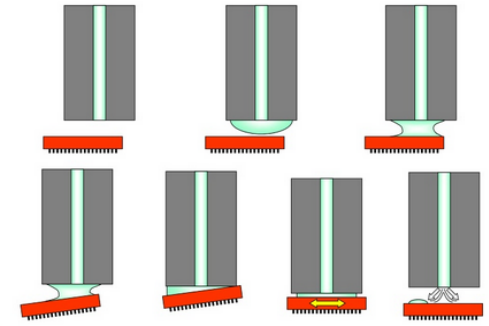

Figure 13 – Capillary micro-grippers

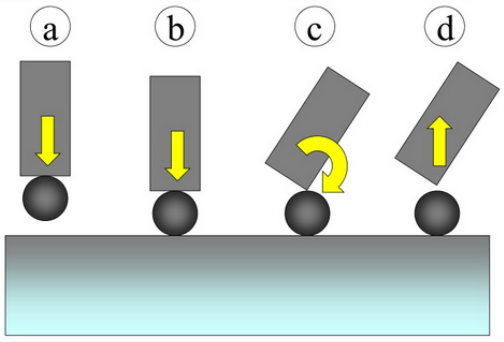

Figure 14 – Van der Waals microgripper functioning

Similarly to capillary force, also Van der Waals forces assumes a complete different importance in micro-world. Sometimes components are so light and small that the only dipoles of molecules of the gripper can carry out the gripping phase: as the tool enters in contact with the component, dipolar forces are relatively induced between the two elements. The contact may cause scratches but is unlikely due to small forces. The grip stiffness and force are not easy to calculate and depends a lot on the materials of both tools and object [11].

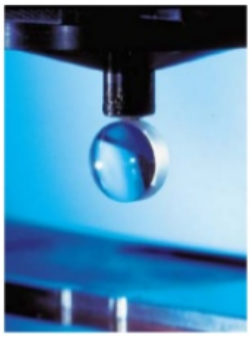

Figure 15 – Cryogenic gripper

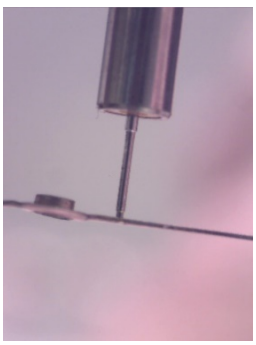

Figure 16 – Vacuum gripper, grasping a clock's hand

However, the grasping mechanism used for this thesis is vacuum. The vacuum gripper consists in a needle in which is created a certain degree of vacuum: the sucked airflow and the pressure difference make the moved object adhere with the end-effector. As other manipulation strategies this one can cause scratches too, but allow great precisions and accuracy and the shape of the object is not a critical factor (exception made for opened structures or porous materials). The grip stiffness depends on the friction while the grip force is retainable along the grip surface. The details of specific grippers used for this work will be discussed in the following chapters.

Finally in certain field is applicable also the so-called phase-transition grippers, that exploit the transition of a material (typically water) from liquid to solid. As reasonable, this technology can't be used with hydrophobic materials and can cause contamination, similarly to capillary end-effectors. The grip force depends upon the material of part, the surface roughness and gripping temperature [5].

2.4.2. CONTACT-FREE MANIPULATION

Contact-free manipulation strategies are very appreciated in those fields where there is a high risk of damaging the object by scratches, deformation or contamination. Due to those reasons, contactless methods are particularly suitable in biomanipulation where samples must be completely isolated from the environment. Moreover, those solutions cancel the problem of sticking effects caused by adhesion's micro-forces.

Bernoulli grippers enters this category and works thanks to air pressures differentials. The incoming compressed air is deflected radially in the gripper and flows back out between the workpiece and gripping surface. The air is routed through a very narrow gap between the end-effector body and the core in the gripper, which greatly accelerate its speed. The high outflow speeds generate a vacuum between the gripper and the workpiece. Spacers hold the object at a distance to ensure that the air can flow off smoothly. As said before exploiting the Bernoulli principle allows to move a wide range of components with a very little contact [12].

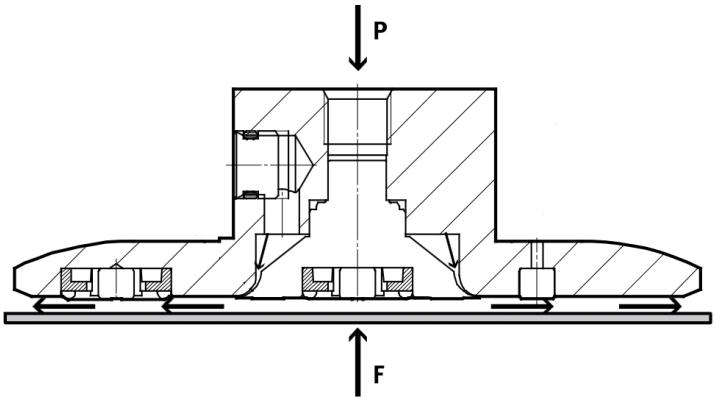

Figure 17 – Contactless Bernoulli gripper air flow

A less conventional approach to obtain contact-less manipulation is achieved using ultrasonic acoustic waves. The working principle of this technology, implies the use of near-field acoustic pressure, which repels the planar object from the gripper surface, while a low pressure vacuum force used to attract it to the same area. An equilibrium point between the repulsive and attractive forces allows the component to levitate about 50 μm below the gripper tip [13] [14].

Figure 18 – Ultrasonic gripper

Other solutions to achieve levitation involve the use of a magnetic or optical tweezer: the former requires electromagnetic fields while the latter use a highly focused laser beam to provide an attractive or repulsive force (typically on the order of piconewtons), depending on the refractive index.

3. ADHESION FORCES

A typical example of robotic application is divided in three phases: pick, transport and place. As explained before, when handled objects weigh some grams the most critical moments are either the pick up or the transport. On the other hand, when parts to be handled are less than one millimetre in size, adhesive forces between gripper and object can be significant compared to gravitational forces, making the releasing part much harder. Those sticking effects can jeopardize the gripping part too, since, for instance, the electrostatic forces can cause the component to jump off the surface into the end-effector as soon as it gets close enough.

Even knowing the theoretical principles and physical phenomena behind those adhesion forces, predict or even measure their intensity is a task far from being simple. As better described in each of the following sections, every phenomenon is greatly influenced by the geometrical shape and by several other variables such as the material (of both gripper and object), the atomic distance between the bodies, the external environment, etc.

3.1. ELECTROSTATIC FORCES

In 1785, Coulomb analysed and studied for the very first time the interaction between charges in vacuum postulating his well-known law.

$$F = \frac{1}{4\pi\varepsilon_0\varepsilon_r}\frac{q_1 q_2}{r^2} \tag{3.1}$$

Where

- ε_0=8.854·10^{-12} F/m is the permittivity of vacuum
- ε_r is the relative permittivity
- r is the distance between the charges

Depending on the sign of the charges, the Coulomb's force may be either attractive (q_1, q_2 discordant) or repulsive (q_1, q_2 concordant). A comparison of the Coulomb's force and the Newton's gravitational force between two charged particles (e.g. a proton and an electron) shows that the electrostatic one is 2.2·10^{39} times greater than the other, due to the smallness of gravitational constant. During the everyday life, electrostatic forces are observable, for example, when films of plastic adhere to other materials, since insulating materials tend to acquire and retain charge [11].

In material media, exist several charged particles with many distributions and dynamics, affecting significantly physical properties of the media. In robotic applications ensuring the perfect relative neutrality between gripper and handled part is very hard. Friction and differences in contact potentials may generate significant amounts of charge, which can be estimated through the Gauss's law (neglecting boundary conditions) [15].

$$\hat{z}\varepsilon_0\varepsilon_r\vec{\mathrm{E}}(\mathrm{z}=0) = \sigma \tag{3.2}$$

With:

- $\vec{\mathrm{E}}$ is the electrical field
- $\hat{z}$ is the surface normal
- σ is the surface charge density [Cm^{-2}]

From equation (3.2), it is possible to obtain the electric field.

$$\vec{\mathrm{E}} \approx \frac{\sigma}{\varepsilon_0 \varepsilon_r} \hat{z} \tag{3.3}$$

$$\mathrm{P} = \frac{1}{2} \varepsilon_0 \varepsilon_r |E|^2 = \frac{1}{2} \frac{\sigma^2}{\varepsilon_0 \varepsilon_r} \tag{3.4}$$

P is known as the electrostatic adhesive pressure for two parallel extended plates, it is measured in pascal, and it is independent of the separation, assuming uniformity of distributed charges. If this last hypothesis decays (non-uniform distribution), the formula would be different and it would depend on distance between surface and gripper. Another important observation to make is that the electric field affects the force more than voltage [11].

The environment influences directly the maximum charge density in a media, for example, at atmospheric pressure and centimetre size gaps, the maximum density for silicon is $\sigma_{max}=3\cdot10^{-5}$ Cm^{-2}. Defining *L* as the length of the side of a silicon cube, it feasible to estimate the smallest cube that will not stick due to electrostatic force.

$$L = \frac{\sigma^2}{2\varepsilon_0 \varepsilon_r \rho_{Si} g} \tag{3.5}$$

When two materials with different contact potential are brought in contact, the charge flows equalizing the potentials. Therefore, theoretically speaking, using conductive end-effectors should reduce the electrostatic sticking effects. However, even the native oxide that covers silicon parts is a very good insulator and can withstand a maximum field strength of up to $3\cdot10^9$ V/m that implies a significant quantity of charge, and considering the equation (3.4) the maximum generable pressure would be about 10^8 Pa (ε_r=3.9) [15].

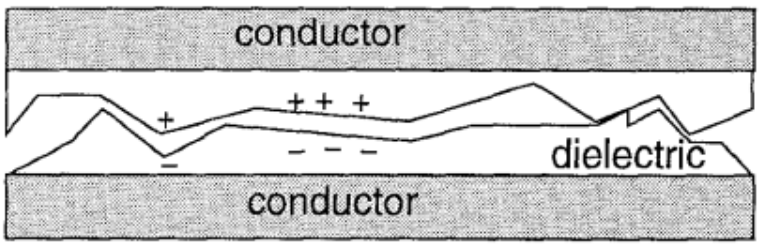

Figure 19 – Disposition of charges between two components in relation with surface roughness

Finally, the surface roughness can influence the stored charge by preventing the equalization of potentials in those regions not in contact, as the picture Figure 19 shows.

3.2. VAN DER WAALS FORCES

As discussed briefly in the previous paragraph, matter is normally electrically neutral. Even if molecules don't possess net charges, they may have a dipole which can be either permanent or inducted, depending if the molecule is symmetric or not. It's important to underline that even symmetrical particles may have some instant dipole caused by the random disposition of electrons. Consequently, several different kind of intermolecular interaction may emerge:

- Ion – dipole interaction force: interaction between a polar molecule and a charged atom that it is strong enough to bind ions to molecules and mutually align them.
- Dipole – dipole interaction force: its intensity depends mostly on the angle between those dipoles. This orientation is not completely random, but those position with lower energy are more probable (according to the Bolzmann's theory).
- Dipole – inducted dipole interaction force.
- Dispersion forces: also called London's dispersions forces that act between all the atoms and molecules. The origin of this dispersion is quantum mechanical and is caused by interaction between instantaneous dipoles.

The contribute given collectively by those last three forces are known as Van der Waals forces. The existence of attractive forces between neutral atoms and molecules gives rise to analogous forces between bodies. In 1937 Hamaker studied the phenomenon, hypothesizing the resultant force between two objects were the sum of all contribution given by each molecule. Under this consideration, Hamaker discovered that there is a significant difference between Van der Waals force in molecules than in material bodies: when single particles are considered, the interaction force decays with the seventh power of distance denoting a very short range of interaction. On the contrary, the force in material bodies decays with the square or cube of the distance (depending on the shape of interacting objects). He created also formulas for Van der Waals force calculation that include a constant called Hamaker's constant. Years later, a number of researchers has

confirmed this assumption of additivity: they obtain the same formulas and equations treating the bodies as continuous media (ignoring their atomic structure), with the only difference of the constant (called Lifshitz's constant) [16].

Finally, about those intermolecular forces is important to underline their strong dependence to materials. For example the attractive effect results greatly reduce when the objects are immerse in a fluid (such as water). Moreover when two metal solids are put in contact with a separation L<1nm, they may form metallic bonds, much stronger than Van der Waals forces.

3.3. CASIMIR EFFECT

This phenomenon was theorised for the very first time by Dutch physicist Hendrik Casimir during his research on the origin of viscous forces. The Casimir effect consists in an attractive force between two solids placed in the vacuum. Its origin is quantum-mechanical. A typical example consists in studying this effect between two perfectly conductive, uncharged plates set in vacuum [8].

$$F_{Casimir} = -\frac{h\, c\, \pi}{480\, L^4}\, A \tag{3.6}$$

The negative sign indicates the attractive nature of the force, which become stronger and stronger as the plates get closer. In the formula:

- h: Plank's constant ($6.62 \cdot 10^{-34}$ Js)
- c: velocity of light in vacuum ($3 \cdot 10^{8}$ m/s)
- A: surface of plates
- L: distance between the plates

Due to the Plank's constant, this force is very small and often negligible [11].

3.4. SURFACE TENSION AND CAPILLARY FORCE

The cohesive forces between liquid molecules are responsible for the phenomenon known as surface tension. This phenomenon is easily observable every time we see an insect striding on the surface of a pond. This happens because liquid's surface has a higher energy than its interior. The capillary adhesion represents an example of how forces with tiny ranges can lead to macroscopic effects [11]. This sticking force depends on the meniscus shape of the liquid between the objects, and often is caused by condensation of water: therefore, relative humidity of the environment plays an important role. In practical situations, hygrometric parameters of air should be kept in check with a relative humidity value at least under the 65%.

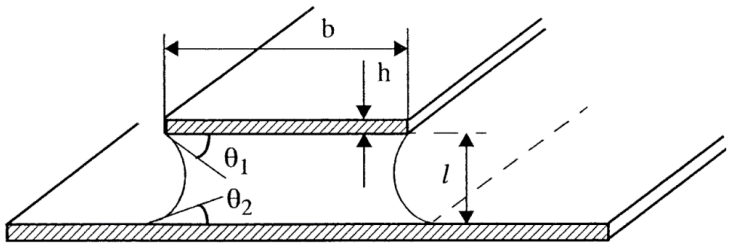

Figure 20 – Liquid meniscus between two parallel planar plates

The image Figure 20 shows an easy example of adhesion caused by those forces: a small film of water separates two planar plates. In this case the force per unit of length value is:

$$F_{Capillary} = -\frac{2\gamma(\cos\theta_1 + cos\theta_2)b}{l} \tag{3.7}$$

The constant γ is the superficial tension and for water (25°C) is 73 mN/m. From the equation (3.7), one could conclude that the range of the force is large, especially if compared to forces analysed in previous paragraphs, since it varies linearly with the length. However, it's important to consider that as the separation increase, the contact angles would increase too with the reduction of the term $(\cos\theta_1 + cos\theta_2)$ [11].

3.5. PRACTICAL EXAMPLE

In this paragraph a practical case will be studied, calculating the principal forces that cause adhesion. The objective of the analysis is to give an idea of the scale of adhesion forces. The objects considered are a gripper, represented by a conductive plane, and the manipulated part by a sphere with radius R = 300 µm and a mass M = 0.125 mg. The image Figure 21 shows the exchange of forces:

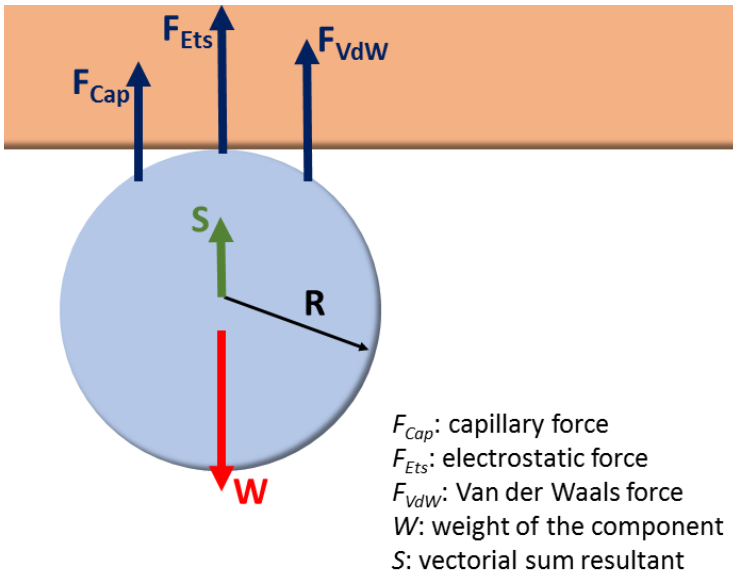

Figure 21 – Scheme of forces exchanged between gripper (orange planar plate) and the manipulated object (blue sphere)

Therefore, the weigh is easy to find: $W = Mg \approx 1.2\ \mu N$.

3.5.1. ELECTROSTATIC FORCE

The electrostatic force in this case, may be calculated with:

$$F_{Ets} = \frac{q^2}{4\pi\varepsilon_r\varepsilon_0(2R)^2} \tag{3.8}$$

The charge in the equation is that of the charged sphere: know its value is not easy since is strongly dependent from the environment and the shape. However, supposing the sphere is made

by a good insulator (e.g. mica) and under standard hygrometric conditions, the charge density may vary from 10^{-6} C/m^2 up to 10^{-2} C/m^2. For the present example, we will consider an intermediate value: $\sigma = 10^{-4}$ C/m^2, that then allows to find the charge:

$$q = \sigma\,(\pi \mathrm{R}^2) \tag{3.9}$$

$$F_{Ets} = \frac{\sigma^2 \pi R^2}{16 \varepsilon_r \varepsilon_0} \tag{3.10}$$

From the (3.10) the electrostatic force results $F_{Ets} \approx 19.9\ \mu N$, that greatly overcomes the weigh. It is important to underline that the density of charge may be not constant on the surface of the sphere and may varies with the environmental conditions too [15] [8].

3.5.2. VAN DER WAALS FORCE

Van der Waals force is not easy to find due to the estimation of its constants:

$$F_{VdW} = \frac{\mathrm{h\ R}}{8\pi l^2} \tag{3.11}$$

Where h is the Lifshitz's constant and z is the atomic separation. This former variable is hard to measure and it depends mostly from the roughness of the surfaces in contact. For the example, supposing smooth areas, $l \approx 100\ nm$, but the results could be much different varying this value since it appears squared in the formula. The Lifshitz's constant rely on other constants:

$$h = \pi^2 C \rho_1 \rho_2 \tag{3.12}$$

With ρ_i are the density of atoms in the two objects and C is called *phenomenological constant* and describes how the molecules of the two materials interact in the medium where they are immerse. In accordance to some experiments made by some researchers of MIT [17] a value for the Hamaker constant the mica in vacuum can be $h = 69.9\ 10^{-21}\ J$, and so the force $F_{VdW} \approx 0.083\ nN$. With the parameters involved, this force is not significant, but the result may be different varying the materials [15].

3.5.3. CAPILLARY FORCE

As discussed in the previous chapter, the formula to find capillary force require the knowledge of contact's angles and surface.

$$F_{Cap} = \frac{\gamma\,(\cos\theta_1 + cos\theta_2)\,S}{l} \tag{3.13}$$

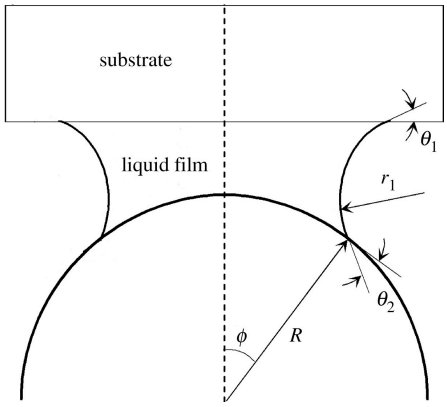

Figure 22 – Film of water between the sphere and the gripper (substrate)

When the separation distance is much smaller than the size of objects and if are considered hydrophilic materials, the formula can be simplify:

$$F_{Cap} = 4\pi R\gamma \tag{3.14}$$

This simplification is reasonable since R is three order of magnitude bigger than l. The final resultant force is $F_{Cap} \approx 275\ \mu N$ [15].

3.6. CONCLUSIONS

The practical example treated in chapter 3.5, is meant to give the reader some sort of "physical sense of magnitude". As seen, the adhesion forces are not always negligible since they can overcome weight hundreds of times. Then, should be evident that estimating the sticking forces is far from being a simple task, since they depend from many parameters: geometric dimensions of

the objects, materials, hygrometric conditions of environment. The small sizes make everything even harder because they limit the approximations. As seen, downscaling the manipulated objects, require a better modelization: parts that seems in contact are separated due to roughness of surfaces, microscopic traces of condensation may jeopardise the ongoing activity… Even knowing all the parameters, the formulas may not be applicable exactly to the studied case. Such approach is reasonable only when the task asked to the robot is unique: in this case an advance model of forces may lead to develop very specific gripping strategies.

4. THE EXPERIMENTAL SETUP

In this chapter, we will describe in detail the experimental settings and all the components used during the development of the thesis. Firstly will be presented the principle of vacuum end-effectors with its advantages and disadvantages; then will follow a detailed description of all the components and tools used explaining, for example, why they were chosen and their peculiarity.

4.1. VACUUM GRIPPERS

Nowadays vacuum grippers are very diffused in microrobotics thanks to their versatility. They normally allow to reach a higher accuracy than the more conventional micro-tweezers because, for example, they need to be in contact with only one surface of the manipulated object (differently by the counterpart based on friction that need at least two). Pliers, to reach high accuracies, need to guarantee as much as possible the symmetry of fingers' movement; this problem, instead, does not affect vacuum end-effectors. Similarly tweezers can cause damages like deformations or scratches on the two surfaces, while vacuum grippers only scratches on a single surface.

Sometimes objects originally designed for different applications, can be used efficiently as vacuum grippers: we will see later in this chapter how glue dispensers or nibs can accomplish the task. So very cheap commercial components can carry out the same task, sometimes even in a better way, of much more expensive and fragile components ad hoc created.

Speaking about the force that a vacuum gripper can generate, is reasonable to think that depends on the grip area and on the pressure difference between its inside and the surface of the object:

$$F_{Grip} = \mathrm{f}(\Delta \mathrm{P}, \mathrm{A}) \tag{4.1}$$

The F_{Grip}, of course, varies with the size of the gripper, but in micro handling applications the actual vacuum degree is in the range of -30 / -80 kPa, which produces the specific grip force of about 0.3 / 0.8 mN/mm^2 [5]. On the other hand, grip stiffness depends on the friction (and therefore materials and roughness) between the gripper and the object.

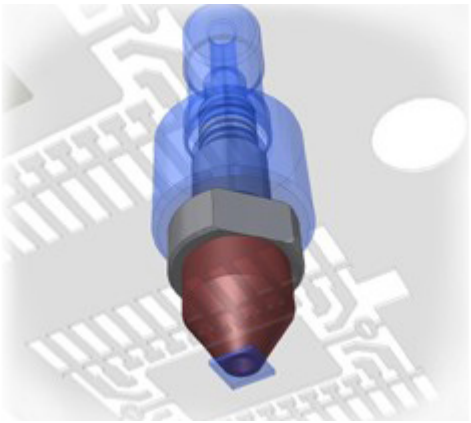

Figure 23 – Example of vacuum gripper: the component is produced by Micro-Mechanics. The picture is a computer reconstruction on how the gripper can grab an electronic circuit.

The negative side of grasping objects from a single surface, is that to lift the heavier components they must be grabbed near their barycentre to guarantee an effective manipulation. But, within a range of weights, this problem is negligible, and even asymmetrical components don't cause troubles. Anyway, a particular caution is required for porous or holed parts: the passage of air through the object make the difference of pressure to fall. Similarly this manipulation strategy is not efficient when moved components are taken in low pressure chambers.

The manipulation through vacuum gripping is particularly appreciated in very fast cycles of production, since the actuation time is minimum (milliseconds).

4.2. ROBOT MITSUBISHI RP-1AH

The studies conducted for this work on end-effectors are not related or dependent from the robot or system used; on the contrary we hope that sooner or later our work will be applied in industrial field and on different machines. However, to be as more complete as possible a brief presentation of the robot is necessary because, so far, the main tests were conducted on it.

The Mitsubishi RP-1AH (Figure 24) is an ultra-compact robot with an arm mass of approximatively 12 kg. Its five-joint are closed in the link structure and the arm section is downsized and made highly rigid, to allow increase of productivity with high-speed operations. It has four degrees of freedom since it can move along the cartesian axis x, y and z, plus the rotation of the end-effector. The positioning repeatability of 0.005 mm has one digit more than the conventional robot and allows to carry out accurate and detailed work [18]. Those performances are achieved thanks to its parallel structure that pledges a high rigidity (essential in those applications).

Figure 24 – Robot Mitsubishi RP-1AH

The last vertical link is a hollow cylinder to allow the air flow inside; as said in the previous paragraph the use of vacuum is very common in micromanipulation strategies. The terminal part of this last link, has a standard ISO M6 screw to attach the grippers and end-effectors more in general. As we'll describe later in this chapter, every gripper used has needed an adaptor to be mounted on the robot.

4.3. VACUUM GENERATOR

In order to use the vacuum as micromanipulation strategy, a vacuum generator is fundamental. Many are the strategies available today on the market to generate a negative (relative to atmosphere) pressure like using different kind of pumps; but in industrial field the most diffused method to carry out the task is to exploit the *Venturi effect*. To accomplish the work we are presenting, we used two vacuum generators based on this effect and produced by the Italian company PIAB: COAX© MICRO Ti05-2 and piINLINE© MINI Si 6-6 mm.

4.3.1. VENTURI EFFECT

When a fluid (in our case air) that is flowing in a duct, meets a restriction of the tube's section, it withstands an acceleration. In fact, for uncompressible fluids in laminar motion, its volumetric flow rate remains constant:

$$Q_v = S\,\bar{V} = Constant \tag{4.2}$$

Where $\bar{V}$ is the average velocity of fluid and S is the section surface of the duct. Basing on the equations (4.2), reducing the diameter of the tube, cause an increase in average velocity [8].

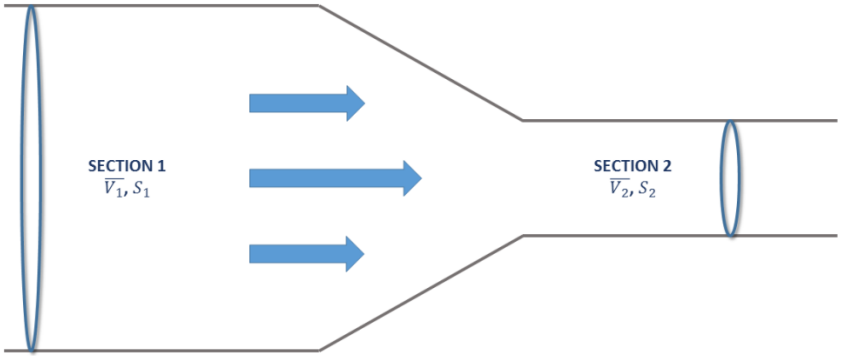

Figure 25 – Duct with a variation in the section. The flow is supposed to be laminar and the fluid uncompressible.

But the change of $\bar{V}$ cause a variation on pressure too: under the same hypothesis of uncompressible fluid and laminar flow, is valid the Bernoulli law (4.3) [19].

$$H = \frac{\bar{V}^2}{2g} + \frac{P}{\rho g} + z = Constant \tag{4.3}$$

The second member of the formula is called *Bernoulli's trinomial*, and ties the average velocity with two other variables: pressure P and height z. Supposing a horizontal tube with a diameter variation the (4.3) becomes:

$$\frac{\bar{V}_1^{\,2}}{2} + \frac{P_1}{\rho} = \frac{\bar{V}_2^{\,2}}{2} + \frac{P_2}{\rho} \tag{4.4}$$

Thus, acceleration of the fluid, involves a decrease in the pressure.

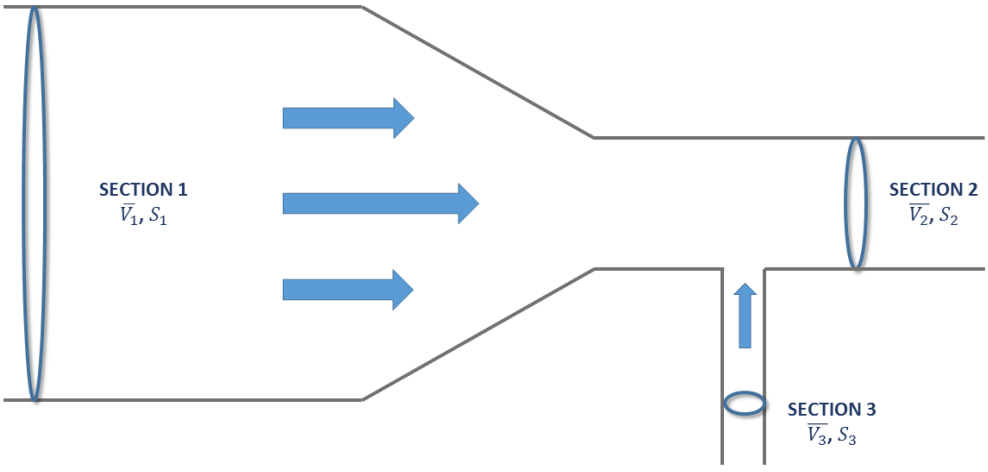

Figure 26 – Venturi effect used to generate a certain degree of vacuum inside a smaller perpendicular tube

The depression we just describe can be used to generate a certain degree of vacuum in a small perpendicular pipe, as the Figure 26 shows. The lower pressure and the high velocity in the section 2, in fact, tend to move for friction the air that lays in the connection between pipes 2 and 3. This movement of air generates, again, a depression in the third section that "pulls" the air contained in it.

4.3.2. COAX© MICRO Ti05-2

One of the vacuum generator used is the COAX© Micro Ti05-2. However, it cannot work alone because it is a cartridge that must be installed in a specific device produced and sold by the same company (PIAB). Many models of this device exist and the one used is the: piCOMPACT10 (Figure 27) [20]. This tool allow the installation of the cartridge and can dock a vacuum gauge and a couple of electro-valves too. Eventually those valves allow to generate an adjustable blow of air as alternative to the releasing mechanism.

Figure 27 – piCOMPACT 10

Figure 28 – Cartridge COAX© Micro Ti05-2

The Figure 29 shows the cartridge that generates the vacuum. The working principle is similar to the one described above: compressed air enters the cartridge (in 1), negative relative pressure is then created (in 2) and finally all the flow exit (exhaust 3) [21].

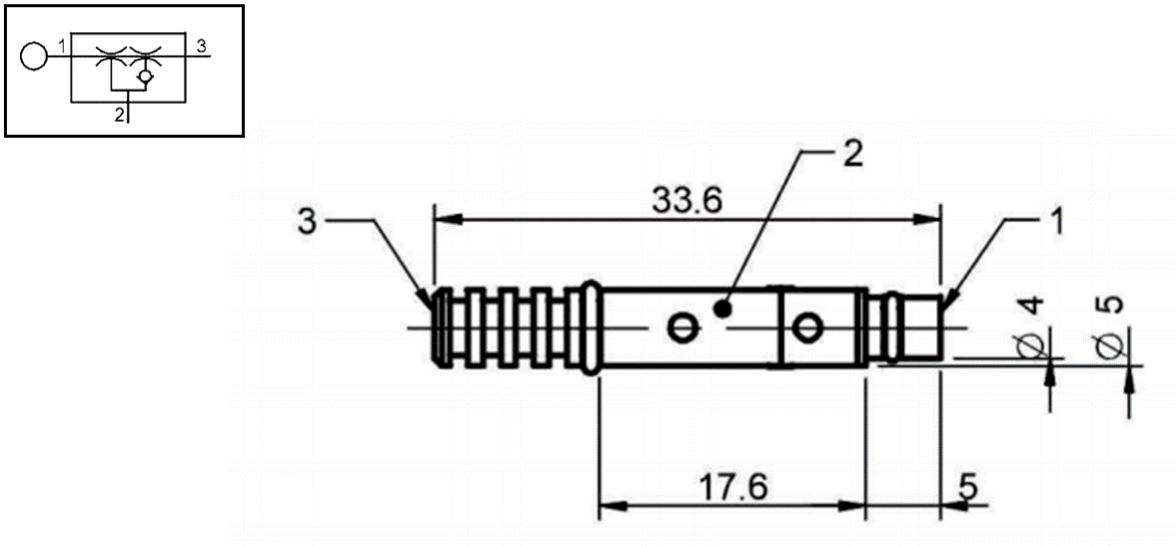

Figure 29 – Dimensions of the cartridge COAX© Micro Ti05-2

The datasheet provided by the manufacturer give us important data: for every measured vacuum degree (-kPa) we can find the sucked airflow rate (Nl/s). Since the device can work with different pressures of air in input, the following graph shows two curves: the blue when P_{in}=4 bar, and the green when P_{in}=6 bar.

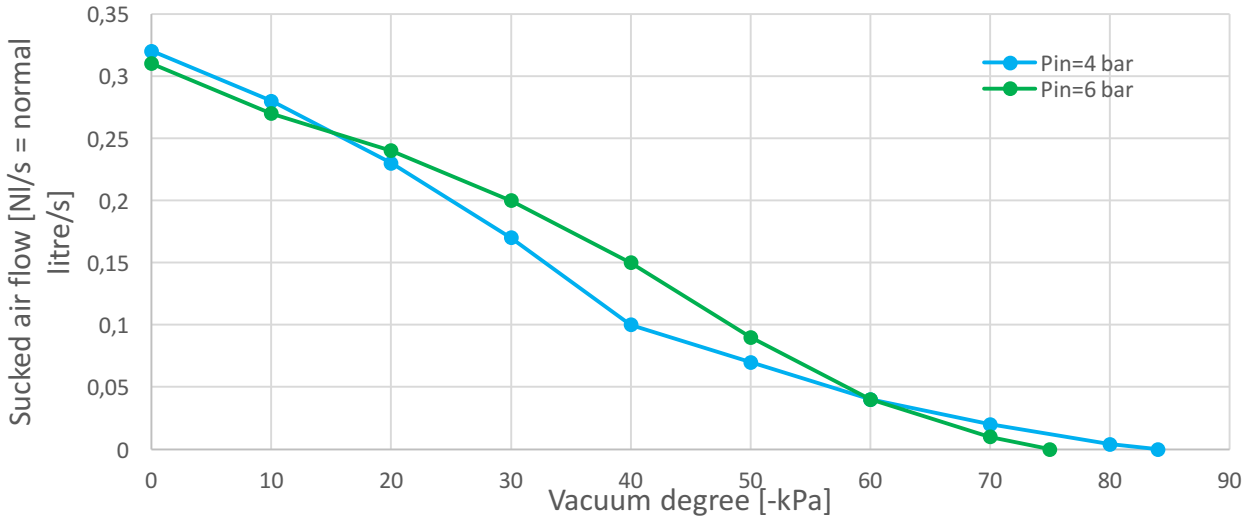

Figure 30 – Characteristic cure of the vacuum generator COAX© Micro Ti05-2

4.3.3. piINLINE© MINI Si 6-6

The second vacuum generator used is the piINLINE Mini Si 6-6 (Figure 31), an extremely compact and ready to use solution. The principal difference, as the name suggests, from the previous product is the possibility to be used alone, with no other components needed. Of course, adding a vacuum gauge or valves, is less convenient in this case, because it would require much more space.

Figure 31 – piINLINE© Mini Si 6-6

The vacuum is formed again thanks to the Venturi effect: looking at Figure 32 the input compressed air enters the section 1, vacuum is generated in section 2 and finally the exhaust exits from section 3.

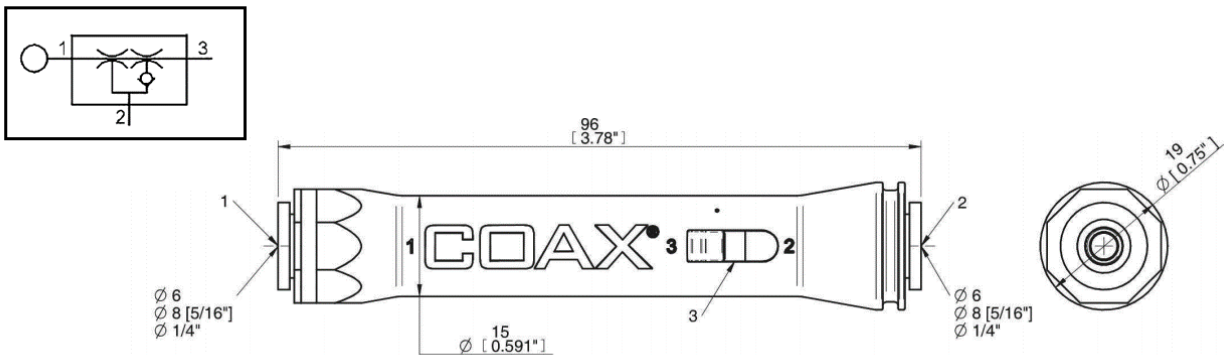

Figure 32 – External dimensions for the piINLINE© Mini Si 6-6 vacuum generator

The producer, again, inserted in the datasheet the characteristic curve of the device, but unluckily for one input pressure only (6 bar). This lack limited in some occasions our work, as we will describe later. However, comparing the following graph with the previous one, it's evident that the shape of the curve is similar, but the sucked air flow is normally higher; the reasons may be the largest ducts that are attached: in this case they measure 6 mm in diameter and 4 mm before (equation (4.2)) [22].

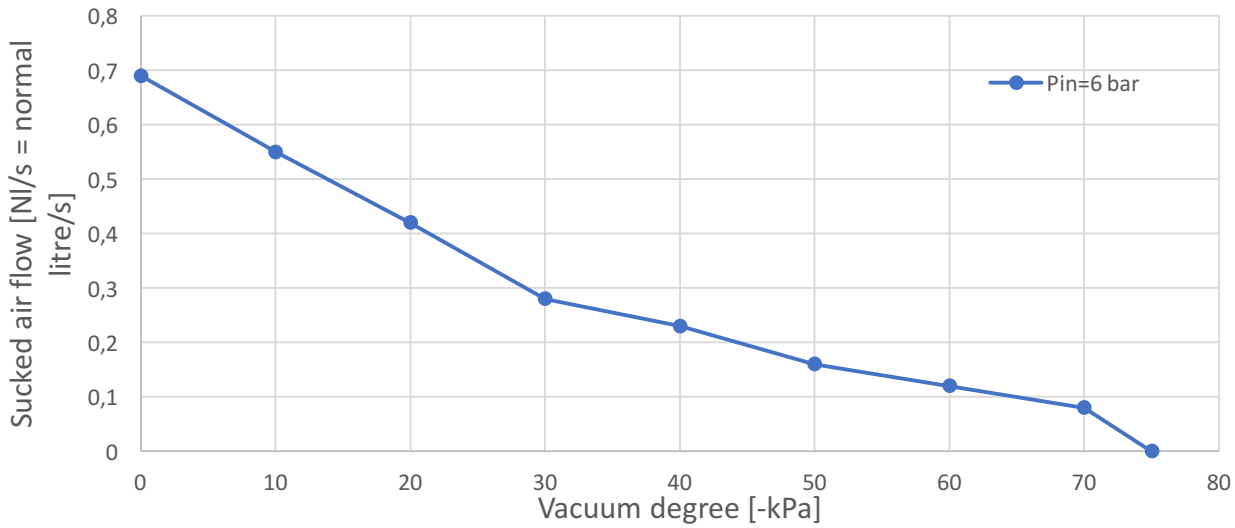

Figure 33 – Characteristic cure of the vacuum generator piINLINE© Mini Si 6-6

4.4. GRIPPING TOOLS USED

During the work for this thesis, have emerged many times the need of establishing a kind of *nomenclature* for some of the components used. Thus, in the following paragraph we will define some names to avoid misunderstandings and will follow a detailed description each gripper used.

4.4.1. NOMENCLATURE

As said, to be clearer some components and subparts require a name. For example since the gripping device presented briefly in the first chapter hasn't a specific name, from now on we will referred to it as *ITIA device* (because was developed in ITIA laboratories) or *dispensing gripper*

(because the producer commercialised it as fluid dispenser) or combinations of those names. Two needles compose this gripper and we will call them:

- The external one: *external, outer,* or *holed needle*, cannula, or *microtube*.
- The internal one: *internal* or *inner needle*.

Finally, the whole structure, internal needle plus the attached weight, will be named *releasing device*.

4.4.2. ITIA GRIPPER

The designers found out that a series of needle produced by E.O.I. Tecne Srl could fit as vacuum gripper after some tests. In fact, their mechanical structure and *flat cut* end make them perfectly suitable to be used as vacuum grippers. They are composed by a plastic body with stainless steel tube. Inside, the cannula is as more uniform as possible because were electrolytically polished, to pledge a homogeneous flow of fluid (in this case air). Before choosing this component they tested some different kind of grippers: an interesting example can be seen in Figure 35.

Figure 34 – ITIA gripper's photograph.

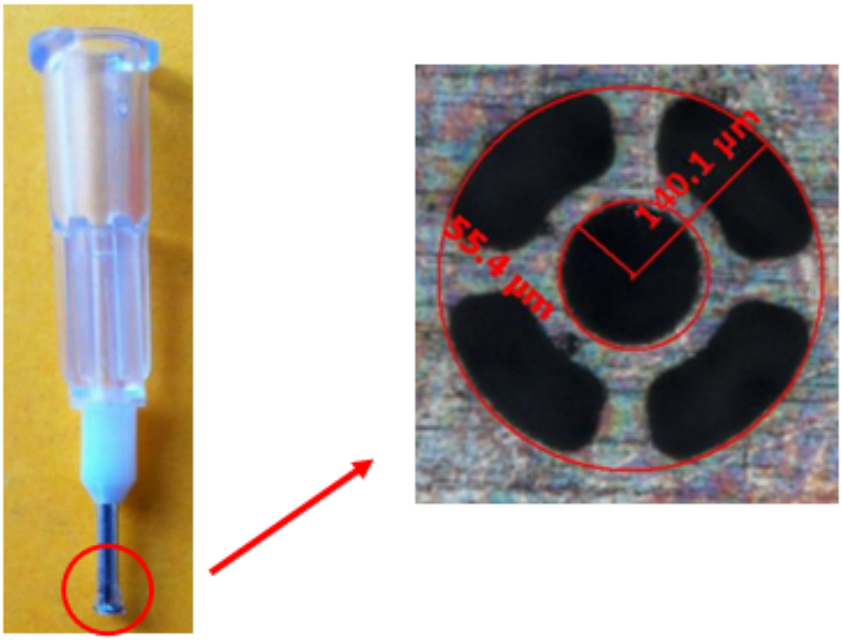

Figure 35 – Unconventional vacuum gripper: its extremity consists in a nozzle with multi-lumina. This end-effector was tested as an alternative to the one used.

The gripper fits a parallelepiped of about 25x10x10 mm^3, but to be mounted on the robot it requires an adaptor; the whole device (adaptor + end-effector) has a volume of 40x10x10 mm^3.

The manufacturer sells those components with different diameters of the cannula: from 1.6 mm to 0.1 mm. In literature, there are only a few studies about the optimal dimensions of the holed needle, but it is possible to demonstrate that the optimum tip size lays in the range between 25% and 50% of the manipulated object [23]. After all, it is reasonable that a larger object requires a larger tip size.

Basing itself on this empirical low, ITIA has chosen the dispensing gripper with 260 µm as internal diameter of the microtube. This measure was taken though a SEM (scanning electron microscope).

As briefly explained in chapter 0, ITIA developed a new kind of releasing mechanism that consists in a small needle surmounted by a small mass that. This component sticks out a little from below, so when the air flows (Figure 36) it is lifted and the manipulated part can be grabbed. As soon as the air flow stops, the releasing mechanism falls heling the detachment.

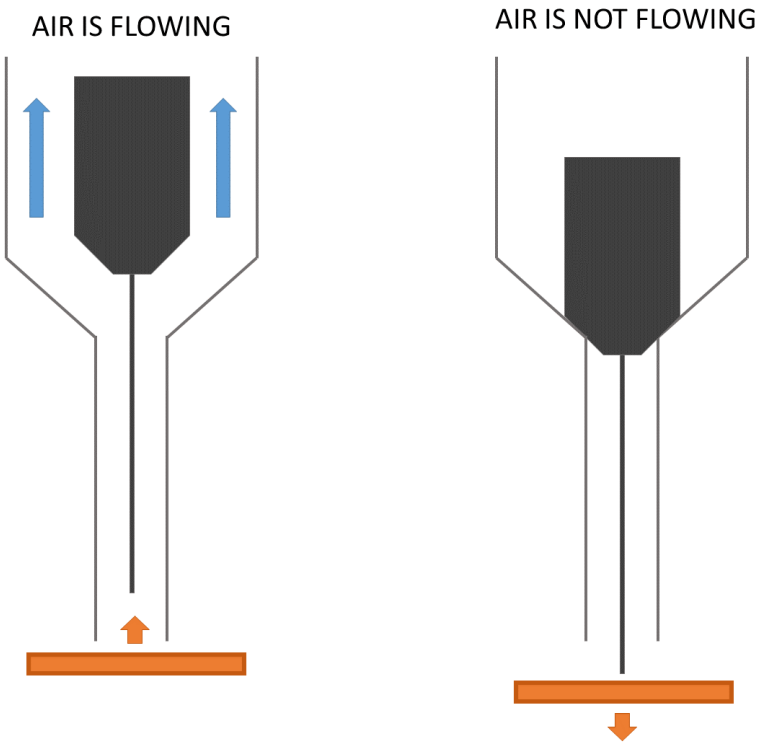

Figure 36 – Functioning scheme for the ITIA gripper

In the following pages the Figure 37, Figure 38 and Figure 39 shows the main dimensions of the device: the first two pictures shows the two components that forms the ITIA gripper, while the last one shows an assembly of the end-effector with its adaptor. About the dimensions specified: most of them have been collected with caliper or SEM, but those concerning the releasing system come from design project.

An electrode originally designed for electro discharge machining has been dimensioned to comply the use of inner needle, since it is particularly well refined. On the other hand, the disk was specifically conceived, designed and prototyped to cover its specific scope; it is made of stainless steel modelled through machining. Some tests were also conducted using a very small pulley from a watch.

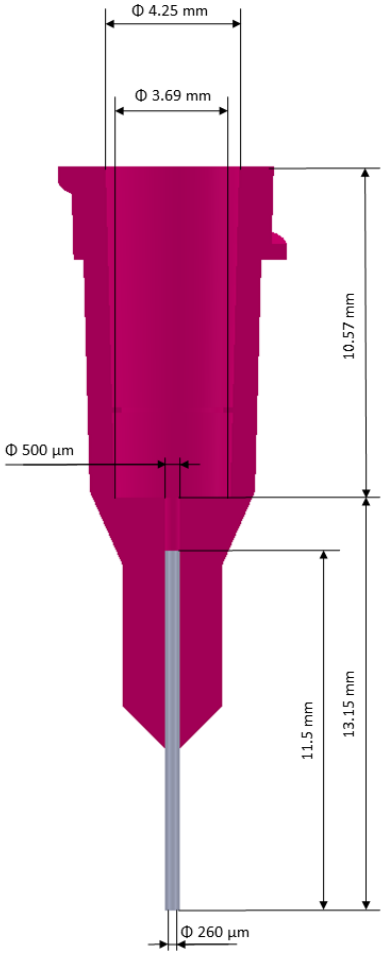

Figure 37 – Section view of the ITIA gripper with its main dimensions specified

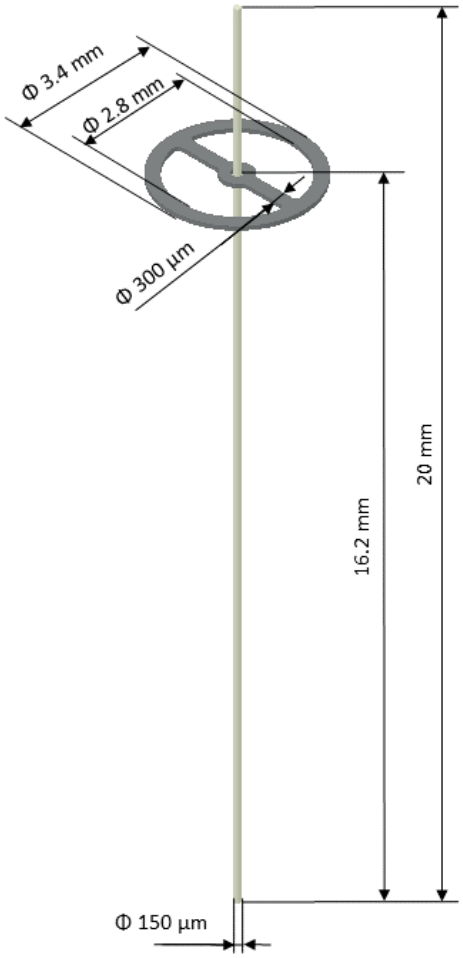

Figure 38 – Releasing device with its main dimensions specified.

The picture Figure 39 in the next page, then, permits to understand more deeply the mode of operation of the device. As suggested by the image, the adaptor (light grey component) not only ensures the stable link between the robot's link and the gripper, but accomplishes a functional role; in fact when the air flows, without this component, the releasing device would be sucked in the vacuum generator. In other words, its internal edge stops the mass and the attached inner needle. The excursion made by the releasing device is 1.2 mm, more than enough to permits the grasping of a component from the gripping end.

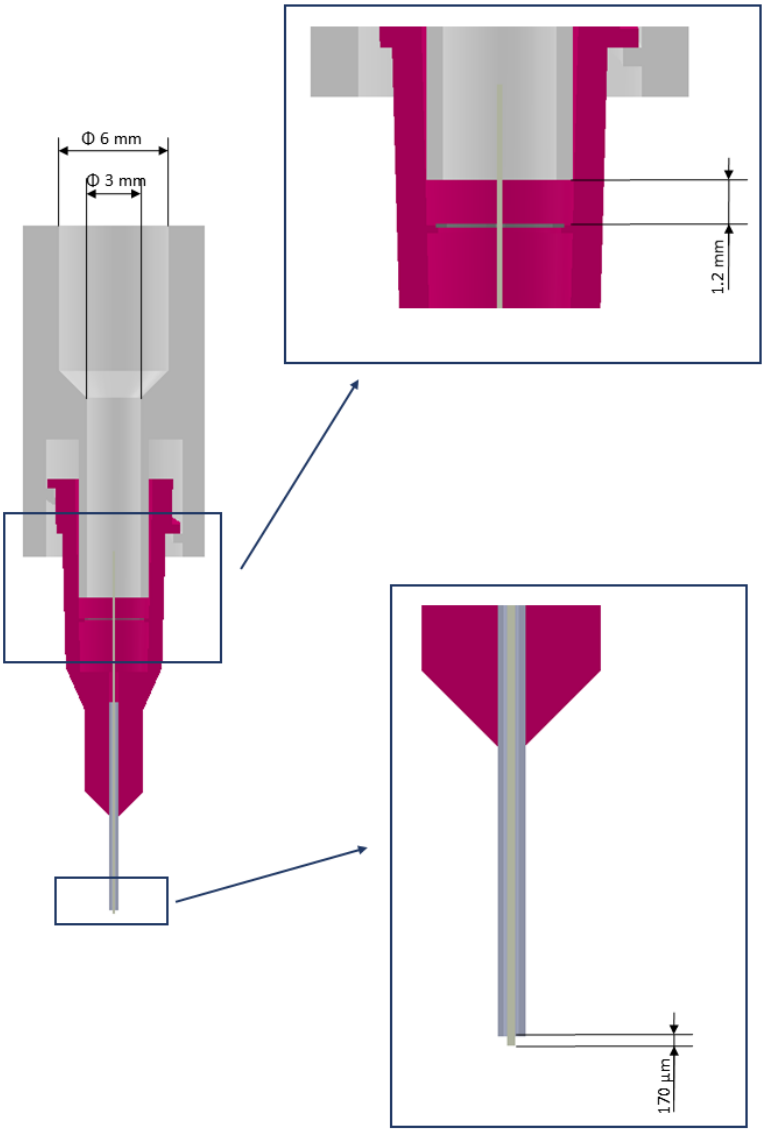

Figure 39 – Assembly of gripper device (including releasing mechanism) with its adaptor. The picture includes the most important dimensions: the excursion of the releasing device, its protuberance from the gripper end and the diameter's variation of ducts inside the adaptor. The upper part will be fastened to the robot through an ISO-M6 screw.

Nowadays exists many grippers that exploits several releasing systems to pledge the 100% detachment, but the innovative aspect of the considered one, is that no additional actuators are involved. As often happens in engineering, the simpler the solution is, the better: such a gripper is light, cheap and easy to repair or replace.

The reader may have notice that all the dimensions specified regard the inner parts of each component; the reason, again, lays in the vast workspace of the robot: outer surfaces don't limit the functionality, while the internal lengths and diameters do.

Finally, we'll spend some words on the mass attached to the inner needle. The weight comply three functions:

- Increase the mass of the needle
- Prevent the aspiration
- Obstruct as less as possible the air flow

The mass represented in Figure 38, consists in a holed disk made of steel with two spokes that links it to its needle. The structure is very light and weighs about 6 mg. The inventors originally design also some lighten variant, such as a transversal bar formed by the two spokes only, for the most delicate operations (high risk of damage).

4.4.3. RAPIDOGRAPH NIB

Unfortunately, the ITIA gripper has some limitation: the mass installed doesn't pledge always the release. Sometimes maybe due to environment, maybe due to the materials in contact, the smallest and lightest manipulated objects do not fall. We would like to underline that the patented device greatly increase the performances if compared to more standard vacuum grippers with more conventional releasing strategies (such as positive air blow). However thinking to industrial reality, if a gripper doesn't release always the components, the production may suffer delays or even suspensions; especially when the operations of the productive process are very fast.

To overcome the problem, a good solution is to increase the mass of the releasing system, at least in those application where the manipulated part is not too fragile. A larger weight and consequently a stronger hit can cause a decrement in performances in terms of accuracy and precision. To bypass this issue, one can think to use a sticking surface (like many companies already do).

A very promising starting point to analyse the impact given by a heavier needle, seemed to be the use of rapidograph (which is a very precise technical pen for drawing) nibs as end-effectors. Similarly to the ITIA grippers, they are composed by a holed cannula and an internal needle with a cylindrical weight on the top. During the normal functioning, as soon as the pen's tip touch the paper, the inner needle (that exits a little bit from the cannula) and its mass are raised unblocking the ink that starts flowing. Since many models that differ for dimensions and geometry exist and

since they are (almost) ready to be used as grippers, the rapidograph seems to be particularly suitable for testing.

The rapidographs initially considered were chosen because already available in the laboratory. Even if those nibs were partially damaged by the wear and, in some occasions, the inner needle was blocked by the dried ink, they have been useful to understand the variation of the cannula and inner needle diameters as function of the line's width of ink (as the graph below shows). In the following diagram two graphs are represented: the blue is relatively to pens produced by the German Rotring, the green by Czech Koh-I-Noor. Of course, the points of each graph indicates the rapidograph tested. Each of those measurements were made with an optical microscope.

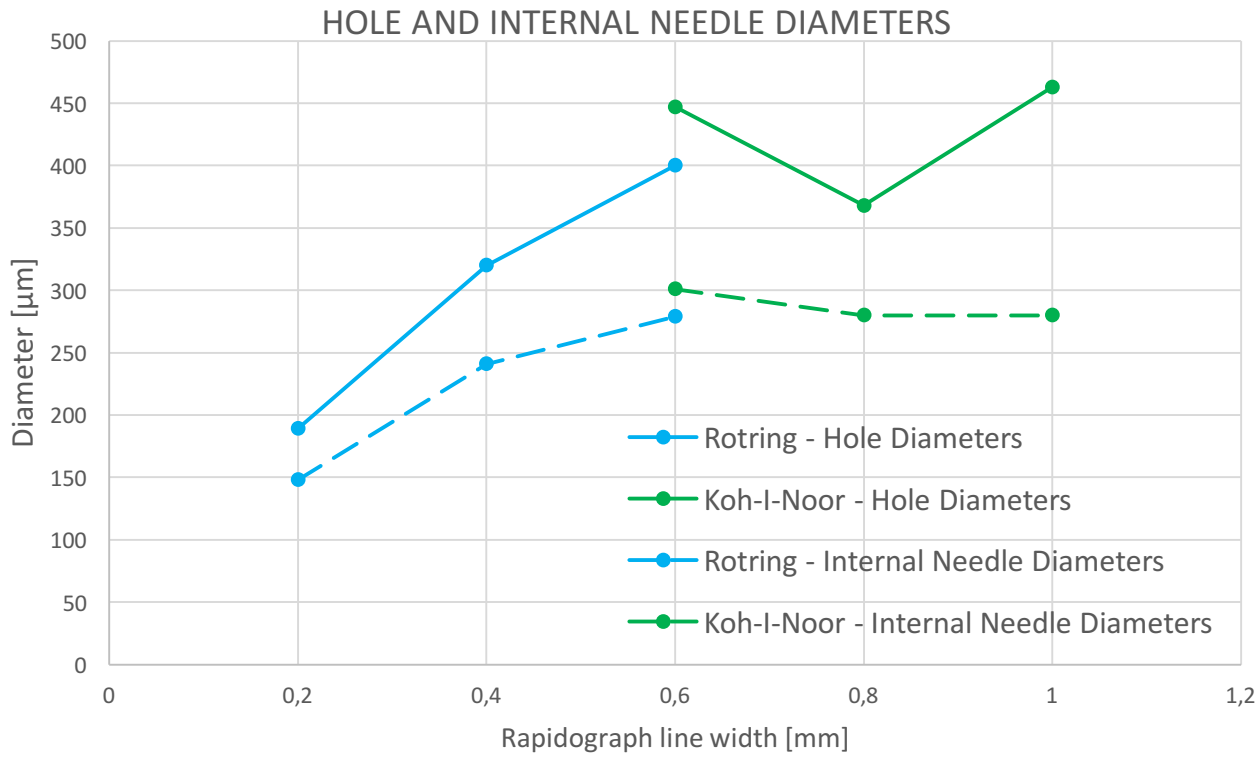

Figure 40 – Cannula's hole and internal needle diameters in relation with the line width of ink. The points stand for the nibs possessed.

The magnification of the microscope highlighted the better quality of Rotring's technical pens; first of all the tips' holes were well refined and much more regular than the Koh's counterparts (Figure 41). Moreover the mass of the internal needle is metallic for Rotring's instruments and made of plastic for the other brand.

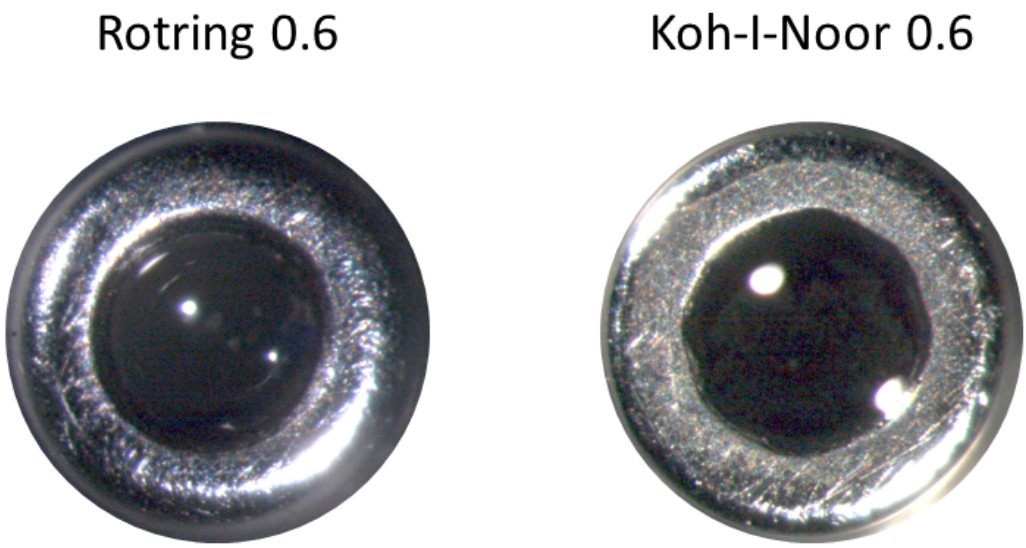

Figure 41 – This image taken from the optical microscope shows a comparison between external needles: one of Rotring the other of Koh-I Noor. The nibs have similar dimensions but the hole on the left is clearly better refined if compared to the one on right (which is not even circular).

As said before, it is possible to demonstrate that the tip for a vacuum gripper should be around the 25-50% of the manipulated component [23]. Since we were evaluating the rapidographs as alternative to the ITIA gripper, we wanted to adopt dimensions as closest as possible. Therefore, reminding that the dimensions for the patented gripper are 260 and 150 µm for the hole diameter and internal needle width respectively, we bought three pens brand new (Figure 42 and Figure 43): the yellow 0.2, the white 0.25 and the green 0.3.

Figure 42 – Rotring rapidographs. From above to below the 0.2, 0.25 and 0.3 nibs.

Figure 43 – The tips can be unmounted and appear like in this photograph.

Figure 44 – Rapidograph inner needle. The mass has the same dimensions for all, while the thinner part varies.

The dimensions of the three tips (Figure 43) are exactly the same, exception made for the hole at the end and the inner needle. Even the mass (Figure 44) that lays on the needle has the same diameter, length and weight. The following table and pictures contain all the most important dimensions: in particular, the figures Figure 45 and Figure 46 show the magnitudes equal from each rapidograph, while the table gives more specific information.

RAPIDOGRAPH			HOLE DIAMETER [µm]	NEEDLE DIAMETER [µm]	MASS WEIGHT [mg]
Rotring Rapidograph	Yellow	0.2	139	79	707
Rotring Rapidograph	White	0.25	152	79	707
Rotring Rapidograph	Green	0.3	208	145	707

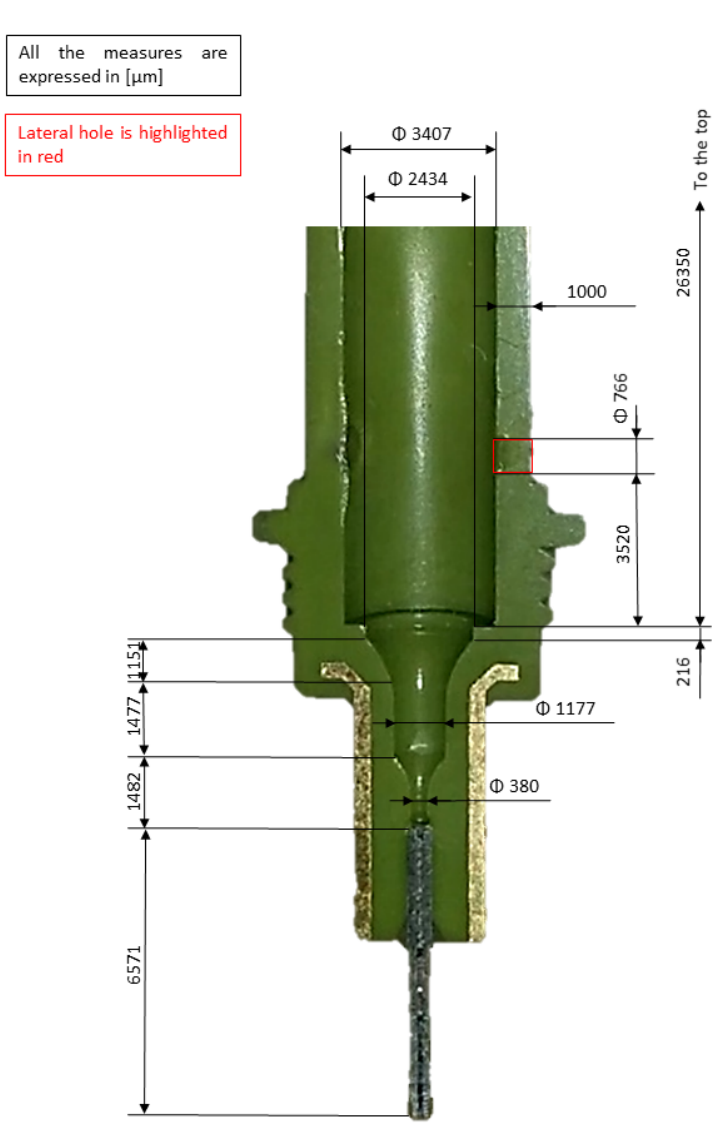

Figure 45 – Photograph of a rapidograph sectioned longitudinally: it was immersed in a transparent resin to keep it steady and then polished until it was half consumed. Measurements reported were taken with an optical microscope.

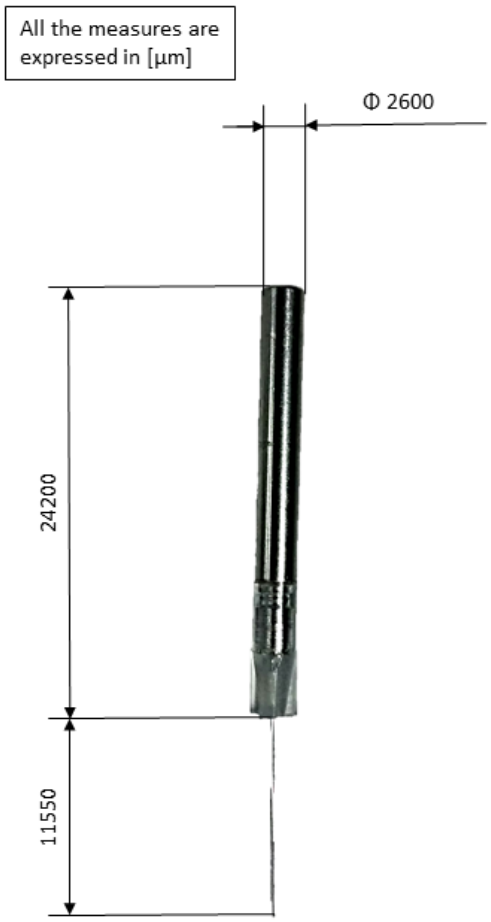

Figure 46 – Photograph of the inner component of a rapidograph. Measurements were taken with a caliper.

As the previous table reports, the mass of our new releasing system is very relevant: 707 mg. This exceed the ITIA's one of two order of magnitude, and so we can expect the release 100 % of times. Rather, the real problem may be lifting the needle and the objects.

We completed the description of the rapidographs but before moving on, we would like to spend some words on an important characteristic. The Figure 43 shows that each technical pen's tip has lateral holes: those two breaches ruins the axisymmetry of the component, but are very important

for the work done. In the picture Figure 45, they are visible, even if not clearly; however their dimensions are indicated.

Finally, like in the previous case, also the rapidographs need an adaptor to be mounted on the robot. Externally the upper part of the pen measures Φ=5.7 mm while the robot ends with an M6 hollow screw.

Figure 47 – Robot-pen adaptor. Made of aluminium the component has an M6 screw in its interior hole, to be attached to robot's end.

5. THE EXPERIMENTAL TESTS

In this chapter, we will present the experiments conducted and the collected data used to develop a theoretical model for the grippers. Those tests are precious for our work: the information found permitted us to gain a good comprehension of the problem.

5.1. INTERNAL NEEDLE LIFTING

In chapter 4.4, we highlighted several times the importance of the lateral holes for the rapidographs, without explaining the reason. The dispenser gripper is completely closed, made exception for the inferior hole where the manipulated component is grabbed. Basing ourselves on this observation we initially sealed the rapidographs' lateral holes; moreover having two additional holes where the air passes through (that are much bigger then the inferior one) make the pressure difference to fall. In fact, remembering the equation (4.1) here reported, i.e. that the gripping force is function of pressure difference, seemed obvious that the lateral holes need to stay closed.

$$F_{Grip} = \mathrm{f}(\Delta \mathrm{P}, \mathrm{A}) \qquad (4.1)$$

Nevertheless, the realising mechanism revealed itself to be too heavy to be lifted. Thus, we had to change strategy. When the air flows, it exerts two different kind of forces on the inner needle:

- A contribute given by the difference of pressure between the inferior part and the superior one.
- A contribute given by the drag, i.e. the friction, of air on the surfaces of the internal component.

Closing the lateral holes maximises the first one and the "lifting power", while removing the obstructions frees the passage for an important air flow rate.

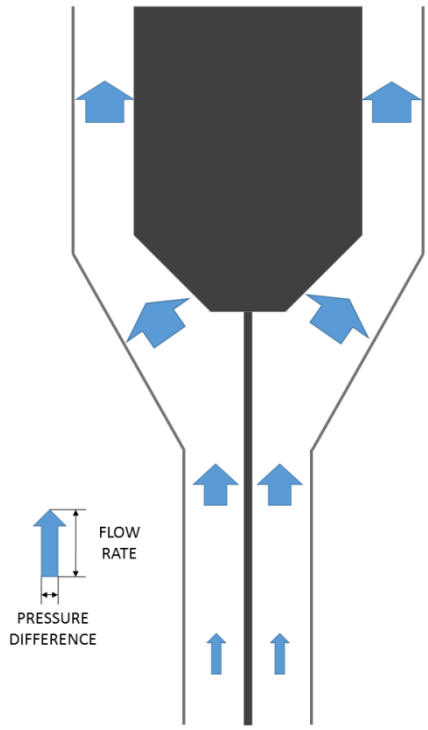

Figure 48 – Maximum difference of pressure: this scheme is meant to give an idea on how the air flows inside the rapidographs' nibs when the lateral holes are sealed. Difference of pressure increase along the duct with constant small flow rate. This is a qualitative scheme.

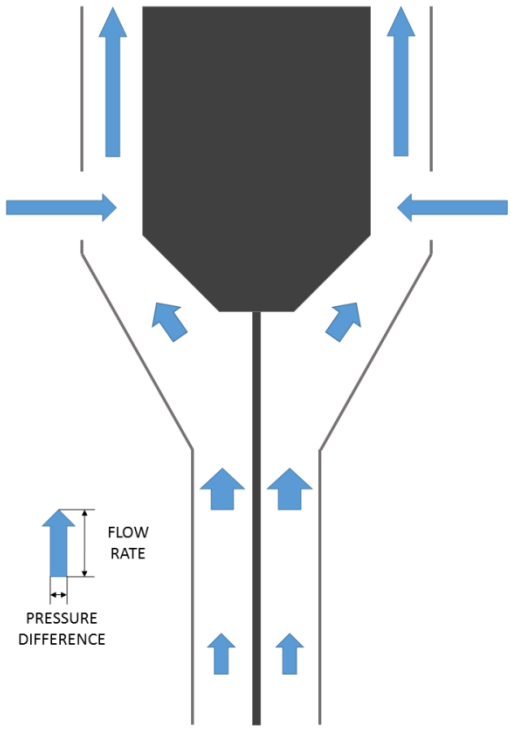

Figure 49 – Maximum air flow: this scheme is meant to give an idea on how the air flows inside the rapidographs' nibs when the lateral holes are fully opened. A huge flow of air passes through them with a small difference of pressure. This is a qualitative scheme.

Experiments proved that leaving the lateral holes fully opened the internal needle was lifted very easily. The side effect was that the remaining difference of pressure between the cannula and the atmosphere was too limited to lift any object.

Those considerations made us understand that probably there was an optimal percentage of obstruction, which guarantees a good trade-off between capability of lifting objects and the inner releasing device. After several attempts we found empirically a good isolation; the Figure 50 shows the results of this research. At first, the complete isolation was carried out by a rubber tube section, which ties very tight the nibs not allowing the passage of air. Then little holes were dug into this rubber tube in correspondence of the lateral holes. Gradually, we increased their size until we were satisfied by the performance.

Figure 50 – Rapidograph in operative conditions: the rapidograph as shown is ready to be used on the robot as end-effector. We invite the reader to notice the little hole dug in the rubber tube in correspondence of the lateral hole of the nib. Such a hole allows enough amount of air to pass and to lift the needle, but not too much (jeopardizing the gripping force). The rubber adhesive tape permits to connect the pen to its adaptor.

The rubber adhesive tape attached on the terminal part of the pen (Figure 50) permits to attach the rapidograph to the adaptor (Figure 47): thanks to its softness the pen can be screwed into the adaptor, practically creating an ISO M6 screw on it. This last solution is not elegant but works fine and it is incredibly easy to apply. If one day, as we hope, our work will be applied in the industrial field, we are confident that a better adaptor will be realised.

We conducted a series of tests to establish the minimum required input pressure to provide to the vacuum generator in order to lift the internal needle. The results reported in the following table are referred to rapidograph in *operative conditions*, i.e. with lateral holes opportunely closed. We also noticed that removing the obstruction of lateral holes, the needle were lifted with 2 bar only.

RAPIDOGRAPH			MINIMUM INPUT PRESSURE [bar]
Rotring Rapidograph	Yellow	0.2	4
Rotring Rapidograph	White	0.25	4.5
Rotring Rapidograph	Green	0.3	4.5

5.2. ASPIRATION TEST

Once discovered the importance of lateral holes we conducted some test to gain an idea on the air flow inside our component. The Figure 51 shows the pneumatic circuit used in ITIA laboratories to carry out those tests. It consists in:

1. The rapidograph nib, opportunely treated as seen in the previous paragraph.
2. A vacuum gauge, very similar to a barometer but with a negative scale of pressure because it measures the relative pressure between atmosphere and the duct ($P_{msrd} = P_{atm} - P_{dct}$).
3. The already described vacuum generator (piINLINE).

Even if not shown in the picture, a pressure regulator permitted to adjust the input pressure in the vacuum generator. A mechanical lock allow the flow of air only when needed.

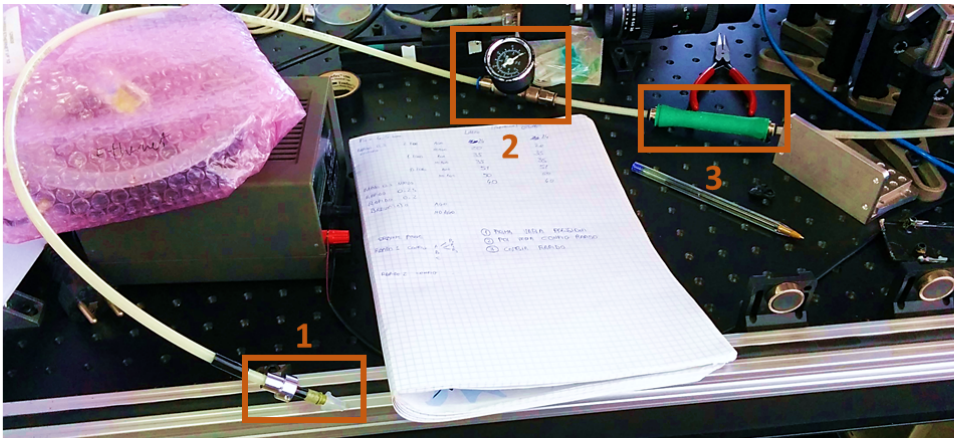

Figure 51 – Pneumatic circuit used in ITIA laboratory to carry out the aspiration tests. 1- Rapidograph, 2- Vacuum gauge, 3- Vacuum generator. This circuit includes also a pressure regulator and a valve that are not present in the photograph, but have a minor importance.

The objective of those tests was to register the vacuum degree (-kPa) changing as much variables as possible. All the data collected are reported in three different tables in the next page.

INPUT PRESSURE: 4.5 bar			Registered Vacuum Degree [-kPa]	
			Inferior hole free	Inferior hole obstructed
Every model indiscriminately	Lateral holes all opened	With needle	24	24
		Without needle	20	20
	One lateral hole opened	With needle	35	35
		Without needle	34	34
	Lateral holes sealed	With needle	51	51
		Without needle	50	50
Rapidograph yellow 0.2	Operative conditions	With needle	38	38
Rapidograph white 0.25	Operative conditions	With needle	45	45
Rapidograph green 0.3	Operative conditions	With needle	40	40
ITIA Gripper		Without needle	51	52

INPUT PRESSURE: 5 bar			Registered Vacuum Degree [-kPa]	
			Inferior hole free	Inferior hole obstructed
Every model indiscriminately	Lateral holes all opened	With needle	29	29
		Without needle	21	21
	One lateral hole opened	With needle	41	41
		Without needle	39	39
	Lateral holes sealed	With needle	57	57
		Without needle	56	56
Rapidograph yellow 0.2	Operative conditions	With needle	43	43
Rapidograph white 0.25	Operative conditions	With needle	50	50
Rapidograph green 0.3	Operative conditions	With needle	45	45
ITIA Gripper		Without needle	58	59

INPUT PRESSURE: 6 bar			Registered Vacuum Degree [-kPa]	
			Inferior hole free	Inferior hole obstructed
Every model indiscriminately	Lateral holes all opened	With needle	26	26
		Without needle	21	21
	One lateral hole opened	With needle	45	46
		Without needle	41	42
	Lateral holes sealed	With needle	65	65
		Without needle	65	65
Rapidograph yellow 0.2	Operative conditions	With needle	49	49
Rapidograph white 0.25	Operative conditions	With needle	56	56
Rapidograph green 0.3	Operative conditions	With needle	51	51
ITIA Gripper		Without needle	65	65

Each table contains the vacuum degree, measured with a specific input pressure (4.5 bar, 5 bar or 6 bar). In all those input conditions, we tried many different configurations:

- Changing the occlusion of lateral holes;
- Removing the internal releasing mechanism;
- Trying to close the inferior needle.

These tests confirm once again the importance of lateral holes: when they are fully closed we have a minimum passage of air, with very similar conditions between the ITIA gripper and our rapidograph nib. In those cases, the pressure difference with the atmosphere is maximum, and consequently we can expect the maximum gripping force; this is actually true only for the patented device because the pen cannot lift its internal component. A second important observation is that the internal needle plays an important role, but only when the difference of pressure is under -60 kPa approximatively. Not only: its importance increase with the increasing of the airflow rate. Finally the input pressure directly modifies the vacuum generated. Unfortunately, the producer of piINLINE does not provide information regarding different input pressures on the datasheet; the flow rate reported is the one with P_{input} = 6 bar.

The data collected, allow the estimation of an important parameter: the occlusion of lateral holes. So far, we said that we *opportunely* or *empirically* closed them, without giving a measure or a percentage of this blockage. The data collected can bridge this gap. We'd invite the reader to look at Figure 52: the three parabolas represented are constructed under different input conditions (4.5, 5 and 6 bar) and are the result of an interpolation between the points drawn as *+*. Those points are the data collected and gathered in the previous tables; they have the vacuum degree as x-axis and the lateral hole's surface as y-axis: since we know their diameter (about 766 µm each), it is easy to calculate their surface when they are fully opened, only one opened or fully obstructed. Instead we don't know (because it is not easy to measure) the unobstructed surface when rapidographs are in *operative conditions*. However, knowing the curves and projecting on them the vacuum degrees registered, we can have an estimation of their openings that have been drawn as little circles. As expected, the circles with the same colour approximately lay on a horizontal line, which indicates that each test report the same value correctly. Not only, we can also establish a range of occlusion levels to make the rapidograph working properly as vacuum gripper. Thus, through a *MatLab* script we calculated the following data.

RAPIDOGRAPH MODEL	AVERAGE OPENING PERCENTAGE RESPECT TO THE MAXIMUM	CORRESPONDENT AVERAGE DIAMETER FOR EACH HOLE
Yellow 0.2	40 %	0.48 mm
White 0.25	19 %	0.33 mm
Green 0.3	34 %	0.40 mm
Average	31 %	0.42 mm

Those values and considerations will be important especially for the future development of the thesis, because it gives an idea on how the nibs must be isolated.

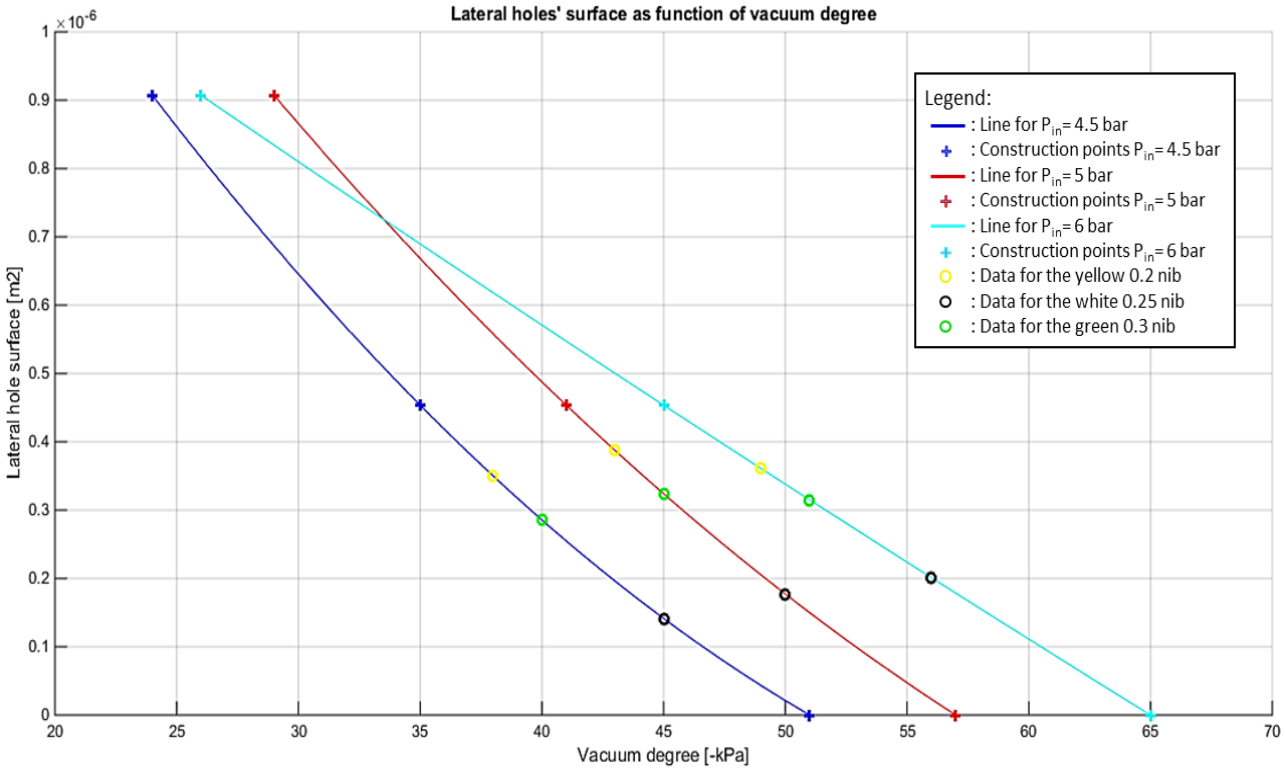

Figure 52 – Estimation of the level of occlusion for the lateral holes. The three parabolas here represented are the result of an interpolation through the points drawn as "+". The coordinates of each point are the vacuum degree for the x-axis and the surface of the lateral holes (when they are fully opened, one open and fully closed) as y-axis. Then, the vacuum degrees for the nibs in "operative conditions" are projected on the curves to find the closure level, here drawn as small circles.

Unfortunately, these tests have some limitations mostly given by the vacuum gauge: its analogic scale lacks of density and it discriminates only the -5 kPa. Due to this fact, some error in reading the value may occurred. However, as seen, the results found are consistent and plausible.

5.3. LIFTING TESTS

To verify the applicability of the rapidograph as vacuum gripper, we decided to conduct a series of lifting tests with some objects of different shapes and masses. Those experiments had the objective to find the limits of the gripper. For each object lifted, we tried different input pressures until we found the minimum to accomplish a safe grasping in order to verify its importance (postulated in the previous paragraph).

The pneumatic circuit used is very similar to the previous one, exception made for the missing vacuum gauge; in addition we used an USB microscope to verify the correct grasping.

In the following photograph (Figure 53) we will present all the objects tested, assigning them a name (for an easier dissertation) and reporting the main characteristics (table in the next page). Then we will present the results of the lifting test.

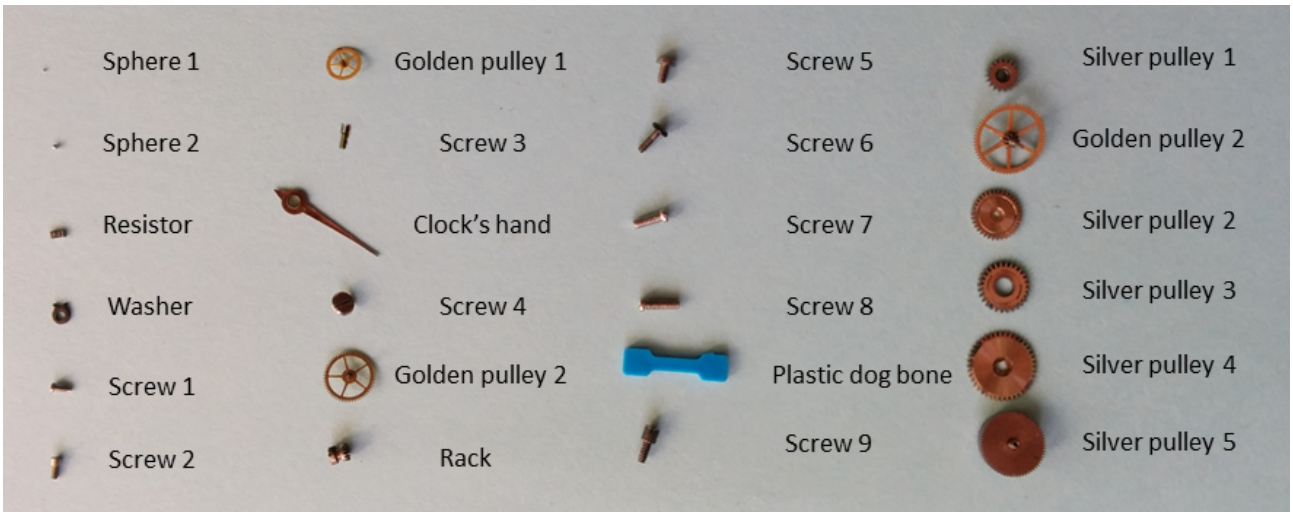

Figure 53 – Samples used for the lifting tests

When we started the tests, we noticed a severe dependency between the lifting capability and the shape (besides the mass). To limit as much as possible the impact of objects' geometry, we used many similar objects (in this case screws) with different masses. Moreover we lifted those components in the same way, i.e. from the tip. By doing this, especially around the threshold between object that can or cannot be lifted, we evaluated only the incidence of the mass.

NAME	MAIN DIMENSIONS [mm]	WEIGHT [mg]
Sphere 1	ϕ = 0.3	0.125
Sphere 2	ϕ = 0.6	1
Resistor	L = 1.6	2
Washer	ϕ = 2.2	5
Screw 1	L = 2.15	6
Screw 2	L = 2.6	8
Golden pulley 1	ϕ = 3.85	9
Screw 3	L = 2.8	14
Clock's hand	L = 13.1	17
Screw 4	ϕ = 2.7	18
Golden pulley 2	ϕ = 5.65	20
Rack	L = 1.9	21
Screw 5	L = 2.85	23
Screw 6	L = 3.8	25
Screw 7	L = 4.0	29
Screw 8	L = 4.45	30
Plastic dog bone	L = 11.6	32
Screw 9	L = 4.05	37
Silver pulley 1	ϕ = 4	42
Golden pulley 3	ϕ = 8	58
Silver pulley 2	ϕ = 5.8	69
Silver pulley 3	ϕ = 6	73
Silver pulley 4	ϕ = 7.8	119
Silver pulley 5	ϕ = 7.2	382

In the next page, the reader can consult the collected data. Obviously, the colours indicate if the objet was or was not lifted successfully: if the slot is red the component could not be grabbed at all, or could be grabbed with a high risk of unexpected detachment. In those last cases the input pressure tried was 7 bar, since this is the operative limit of the vacuum generator. The data are organised in three main groups each correspondent to a different rapidograph model and each with the minimum input pressure specified.

RAPIDOGRAPH	YELLOW 0.2			WHITE 0.25			GREEN 0.3		
OBJECT	LIFT?	DETACH?	Minimum P_{in}	LIFT?	DETACH?	Minimum P_{in}	LIFT?	DETACH?	Minimum P_{in}
Sphere 1	yes	yes	4	yes	yes	4.5	yes	yes	4.5
Sphere 2	yes	yes	4	yes	yes	4.5	yes	yes	4.5
Resistor	yes	yes	4.5	yes	yes	4.5	yes	yes	4.5
Washer	yes	yes	4.5	yes	yes	5	yes	yes	4.5
Screw 1	yes	yes	4.5	yes	yes	4.5	yes	yes	4.5
Screw 2	yes	yes	5	yes	yes	4.5	yes	yes	4.5
Golden pulley 1	yes	yes	5	yes	yes	4.5	yes	yes	4.5
Screw 3	yes	yes	5	yes	yes	5.5	yes	yes	5.5
Clock's hand	yes	yes	5.5	yes	yes	5	yes	yes	4.5
Screw 4	yes	yes	4.5	yes	yes	4.5	yes	yes	4.5
Golden pulley 2	yes	yes	5	yes	yes	4.5	yes	yes	4.5
Rack	yes	yes	5.5	yes	yes	5	yes	yes	4.5
Screw 5	yes	yes	5.5	yes	yes	5.5	yes	yes	4.5
Screw 6	no		7	no		7	yes	yes	4.5
Screw 7	no		7	no		7	yes	yes	5.5
Screw 8	no		7	no		7	yes	yes	5.5
Plastic dog bone	no		7	no		7	no		7
Screw 9	no		7	no		7	no		7
Silver pulley 1	no		7	no		7	no		7
Golden pulley 3	no		7	no		7	no		7
Silver pulley 2	no		7	no		7	no		7
Silver pulley 3	no		7	no		7	no		7
Silver pulley 4	no		7	no		7	no		7
Silver pulley 5	no		7	no		7	no		7

Looking at the results, it seems that the samples were collected opportunely, in fact no red lines are mixed with green ones; that means that the lifting threshold is clear and that it depends only on the mass variation.

An important observation for our work is that in no occasion the component stayed attached to the gripper and the release, at least in those tests, occurred on the 100 % of times.

Finally, the experiment partly rejects the important role of input pressure. At least when we focus on the manipulated components, all the liftable samples have minimum input pressures inside a range of 1 bar, while the too heavy parts cannot be moved even raising to the maximum this parameter. Therefore, changing the input pressure make the vacuum degree to vary, but it doesn't affect much the lifting threshold.

5.4. ACCURACY AND REPETABILITY TESTS

We decided to mount the rapidograph green nib (in operative conditions) on the Mitsubishi robot with its already described adaptor. The idea was to accomplish some pick and release tasks as an ultimate experimental test. Since the robot, when operates with the ITIA gripper, uses the vacuum generator COAX Micro, we repeated the internal needle lifting test using that cartridge. Nevertheless, as we already underlined (4.3.3), this device has a much smaller flow rate when compared to the piINLINE Mini; so reduced that the test failed. In the following chapters (6.3), we will explain the importance of the flow rate for the rapidograph nib. Therefore, we decided to carry out the pick & place tasks with the piINLINE vacuum device, even if this means changing the usual pneumatic circuit.

5.4.1. REPEATABILITY AND ACCURACY TESTS

In this section, we will explain how repeatability and accuracy tests were carried out. First of all, a series of preliminary tests revealed that results directly depend on the complexity of trajectory: e.g. a movement along the z-axis only, leads to an easier release than a movement along two or three axis. Therefore, a trajectory more similar to the path of a real pick and place operation (multi axial movement) was adopted for the tests. The objects moved are a small resistor and a tin sphere, since the same objects were used for a series of similar pick and place tasks with the ITIA gripper. Our purpose, in fact, is to produce comparable data with those two grippers. The tests were composed by many pick and place cycles to guarantee a statistical significance. Every repetition consisted in:

- The vision system takes an image of the component on the substrate. Then some algorithms recognise it in the field of view and calculate the position's coordinates.
- The robot uses those coordinates to move over the component and grab it, switching on the vacuum pump.
- The robot realises some movement along x-y-z axis, then it goes to a predefined release position.
- The camera takes a second picture of the object just before the release and again the computer finds its coordinates.

- The vacuum generator is switched off, releasing the component.
- The camera takes a third picture to the object on the substrate and computes the position.
- The releasing distances are calculated through the difference of coordinates between the second and third photographs.

The input pressure to the system was 6 bar with an environmental temperature of about 20°C [24].

5.4.2. TESTS WITH THE RESISTOR

The resistor in Figure 54 was used as a first object to accomplish those preliminary tests. It measures 1.5 x 0.8 x 0.45 mm with a mass of 2 mg and it was chosen because its shape is particularly suitable to evaluate changes in orientation or overturning.

Figure 54 – Photograph of the resistance used for the repeatability and accuracy tests

In particular, we lifted this component 40 times with the green rapidograph and we will compare the accuracy and repeatability to the 30 pick and place done with the ITIA gripper. The releasing height respect to the horizontal substrate is 150 µm. The following table reports the results of accuracy and repeatability (in both positioning and orientation) for the two end-effectors.

GRIPPER	ACCURACY		REPEATABILITY	
	In positioning [mm]	In orientation [°]	In positioning [mm]	In orientation [°]
Green Rapidograph	0.077	-2.493	0.699	26.639
ITIA Gripper	0.057	2.478	0.595	45.759

During those tests, the release was carried out the 100% of times. Unfortunately those tests seem to confirm a deterioration of performances in positioning with a slightly improvement in orientation. The worsening of 20 µm for accuracy and more than 100 µm for the repeatability is mostly caused by the much heavier internal release mechanism. While the ITIA gripper's one

weighs about 5 mg, ours has a mass of 707 mg (about $1.5 \cdot 10^2$ times heavier). Nevertheless, we think that a further analysis may be interesting, because such a needle should always guarantee the release and the deterioration of performances can be balanced with the application of an adhesive substrate [25].

5.4.3. TESTS WITH THE SPHERE

The sphere used for those tests is the same described in paragraph 5.3, i.e. a tin sphere with a diameter of 600 µm (Figure 55).

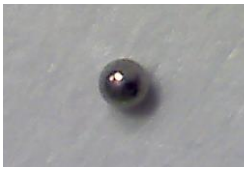

Figure 55 – Photograph of the tin sphere (Φ=600 µm). Taken with an USB microscope.

Unfortunately, in this case the collected results for the green rapidograph are terrible, since many times the sphere was released several millimetres (sometimes even centimetres) far from the releasing point. We conducted 30 repetitions and in 6 occasions, the sphere was "shot" out of the field of view. The reason of this behaviour probably is related to asymmetries: if for example the internal needle is not exactly in the middle of the cannula, when the releasing mechanism falls it does not hit the sphere in its centre causing a lateral translation (like in the game of pool). Of course, the heavier the mechanism the bigger the lateral movement. Those results are very different from the ones found for the resistor: we can therefore conclude that the rapidograph can be used only when the manipulated components have planar surfaces.

6. FLUID DYNAMICS ANALYSIS

As said in the 3rd chapter, approaching the study of our vacuum grippers and their releasing mechanisms under the adhesive forces point of view is not convenient. The great number of variables involved, make the approach not suitable for general treatment. An alternative method may be the study of the fluid dynamics that describes the behaviour of airflow inside our components. In this chapter we will try to follow this approach starting with a brief introduction about the required fluid dynamics theory.

6.1. THEORY'S HINTS

In physics, the *Navier–Stokes equations* describe the motion of viscous Newtonian fluids. These momentum balance equations arise from applying Newton's second law to fluid motion, together with a constitution relation that relates the stress in a fluid to a diffusing viscous term and a pressure term. Navier–Stokes equations are useful because they describe the physics of many phenomena of scientific and engineering interest [8].

$$\begin{cases} \frac{d\rho}{dt} + \nabla \cdot (\rho \boldsymbol{q}) = 0 \\ \rho\left(\frac{d\boldsymbol{q}}{dt} + \boldsymbol{q} \cdot \nabla \boldsymbol{q}\right) = -\nabla p + \nabla\left(\mu(\nabla \boldsymbol{q} + (\nabla \boldsymbol{q})^{\boldsymbol{T}}) - \frac{2}{3}\mu(\nabla \cdot \boldsymbol{q})\boldsymbol{I}\right) + \boldsymbol{F} \end{cases} \quad (6.1)$$

In (6.1) the second equation is the Navier-Stokes equation while the first one is the *continuity equation*, which express conservation of mass. In (6.1) the variables are the fluid velocity $\boldsymbol{q}$, the pressure p, and the density ρ. μ represents the dynamic viscosity a fluid property, whereas, $\boldsymbol{F}$ is the resultant of the external forces per unit of volume acting on the fluid (e.g. weight force). If the fluid can be considered incompressible, e.g. ρ is constant, equations (6.1) form a closed system of equations; otherwise it must be supplemented by the energy equation and the equation of state.

Those equations are non-linear and it doesn't exist a general method for their solution. Every new problem must be formulated carefully for what concerns the geometry choices and the better boundary conditions; then a procedure to follow must be studied, hoping to find a solution. Many times the exact solution is not available and so numerical (approximated) solutions must be exploited. However, in a few cases, due to some simplifications, an exact solution can be found. Now we will present a couple of those cases, all considering laminar flows [26].

6.1.1. CURRENT IN A CIRCULAR DUCT

First of all we will consider a circular duct with axis of symmetry along the z-axis and radius R, filled with incompressible fluid in both directions $\pm z$. The following boundary conditions are applied:

$$\boldsymbol{q} = 0 \text{ for } r = R \quad (6.2)$$

Where $\boldsymbol{q}$ is the velocity vector and r is the radial coordinate. The imposed boundary condition is called *no-slip* condition. We assume complete axis-symmetry around the z-axis. As a first assumption, we will postulate that the velocity vector has only one component different from zero, the one parallel to z-axis. If a consistent solution will be found, it will mean that this assumption is correct and that the flow is monodirectional.

$$q_r = q_\theta = 0 \text{ everywhere} \quad (6.3)$$

The continuity equation expressed in cylindrical coordinates is:

$$\nabla \cdot q = \frac{1}{r}\frac{\partial}{\partial r}(rq_r) + \frac{1}{r}\frac{\partial}{\partial \theta}(q_\theta) + \frac{\partial}{\partial z}(q_z) = 0 \tag{6.4}$$

Because of equation (6.3):

$$\frac{\partial q_z}{\partial z} = 0 \tag{6.5}$$

thus:

$$q_z = w = w(r, \theta) = w(r) \tag{6.6}$$

Where dependence on θ is neglected to enforce a complete symmetry around the z-axis. Navier-Stokes equations, under stationary conditions, becomes:

$$\begin{cases} 0 = \dfrac{\partial P}{\partial r} \\ 0 = \dfrac{1}{r}\dfrac{\partial P}{\partial \theta} \\ 0 = -\dfrac{\partial P}{\partial z} + \dfrac{\mu}{r}\dfrac{\partial}{\partial r}\left(r\dfrac{\partial w}{\partial r}\right) \end{cases} \tag{6.7}$$

Where $P = p + \rho g h$ is the modified pressure: it is very useful in hydrodynamics but it can be used only with the density constant and when the pressure *p* does not appear in boundary conditions. P varies with *z* only, but rewriting the last equation of (6.7)

$$\frac{\partial P}{\partial z} = \frac{\mu}{r}\frac{\partial}{\partial r}\left(r\frac{\partial w}{\partial r}\right) = const \tag{6.8}$$

It is easy to notice that the first member does not depend on *r* and the second does not depend on *z*. Therefore to be equal, they must necessarily be constant. So we have that:

$$\frac{1}{\mu}\frac{dP}{dz} = \frac{1}{r}\frac{d}{dr}\left(r\frac{dw}{dr}\right) \tag{6.9}$$

The integration leads to the general result:

$$w(r) = \frac{1}{4\mu}\left(\frac{\Delta P}{\Delta z}\right)r^2 + C_1 + C_2\, ln\,(r) \tag{6.10}$$

For a current in a circular duct with radius *R* and applying the boundary conditions:

$$w(r) = -\left(\frac{\Delta P}{\Delta z}\right)\frac{R^2}{4\mu}\left[1 - \left(\frac{r}{R}\right)^2\right] \tag{6.11}$$

The sign indicates that the flow is directed towards lower values of the modified pressure. In correspondence of the axis of the duct, the velocity (maximum) is:

$$w_0 = -\left(\frac{\Delta P}{\Delta z}\right)\frac{R^2}{4\mu} \tag{6.12}$$

$$w(r) = w_0\left[1 - \left(\frac{r}{R}\right)^2\right] \tag{6.13}$$

The volume flow rate is obtained upon integration of the velocity across a duct section:

$$Q = \int_0^R w(r)2\pi r\, dr = \int_0^R w_0\left[1 - \left(\frac{r}{R}\right)^2\right]2\pi r\, dr = \frac{1}{2}\pi R^2 w_0 \tag{6.14}$$

and, considering equation (6.12):

$$Q = -\frac{\Delta P}{\Delta z}\frac{\pi R^4}{8\mu} \tag{6.15}$$

The equation (6.15) is known as *Poiseuille equation*. The average velocity can be found as:

$$\overline{w} = \frac{Q}{A} = -\frac{\Delta P}{\Delta z}\frac{R^2}{8\mu} \tag{6.16}$$

6.1.2. CURRENT IN A RING-SHAPED DUCT

Making the same considerations just shown, we can find something similar to equation (6.10) for the flow in a ring-shaped duct. The boundary condition, however, are different even if similar. We will consider of stationary two coaxial cylinders are stationary with the fluid motion caused by a difference of pressure along the z-axis exists (Figure 56) [26]. The boundary conditions are:

$$w = 0 \quad \text{for} \quad r = R_e \tag{6.17}$$

$$w = 0 \quad \text{for} \quad r = R_i$$

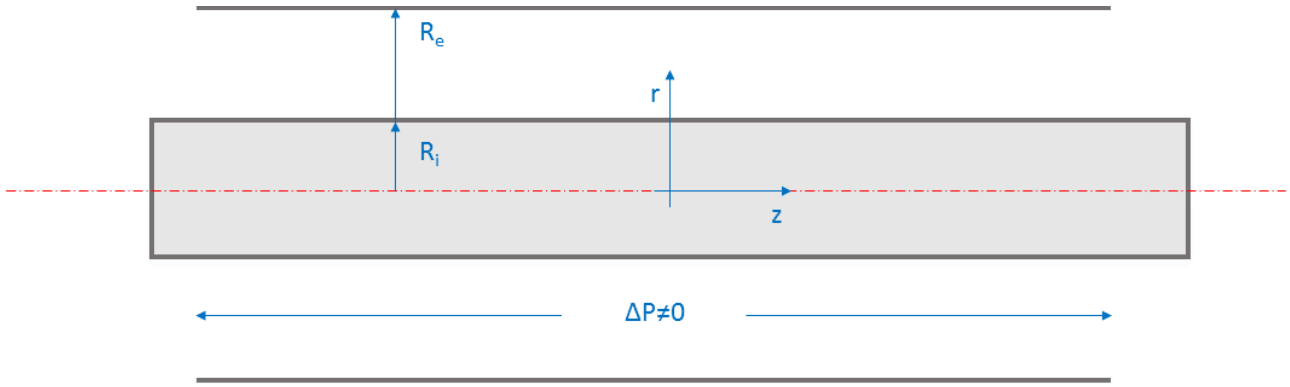

Figure 56 – Ring-shaped duct: a difference of pressure along the duct causes the fluid in motion.

The equation (6.10) in this case gives a different fluid velocity distribution.

$$w(r) = -\frac{\Delta P}{\Delta z}\frac{1}{4\mu}\left[(R_e^2 - r^2) - (R_e^2 - R_i^2)\frac{ln\left(\frac{r}{R_e}\right)}{ln\left(\frac{R_i}{R_e}\right)}\right] \tag{6.18}$$

Setting the first derivative equal to zero is possible to find the maximum velocity.

$$\frac{\partial w(r)}{\partial r} = -\frac{2r}{R_e^2} - \left[1 - \left(\frac{R_i}{R_e}\right)^2\right]\left(\frac{\frac{1}{r}}{ln\left(\frac{R_i}{R_e}\right)}\right) = 0 \tag{6.19}$$

$$\left(\frac{r}{R_e}\right)^2 = \frac{1 - \left(\frac{R_i}{R_e}\right)^2}{2\ln\left(\frac{R_i}{R_e}\right)}$$

Which can be substituted in (6.18) to find the maximum velocity:

$$w_0 = \left(-\frac{\Delta P}{\Delta z}\right)\frac{R_e^2}{4\mu}\left[1 - \frac{1 - \left(\frac{R_i}{R_e}\right)^2}{2\,ln\left(\frac{R_i}{R_e}\right)}\left(1 + ln\frac{1 - \left(\frac{R_i}{R_e}\right)^2}{2\,ln\left(\frac{R_i}{R_e}\right)}\right)\right] \tag{6.20}$$

This velocity distribution is the Poiseuille flow in a ring-shaped duct. The volumetric flow rate:

$$Q = \int_{R_i}^{R_e} w(r) 2\pi r \, dr = \left(-\frac{\Delta P}{\Delta z}\right) \frac{\pi R_e^4}{8\mu} \left[1 - \left(\frac{R_i}{R_e}\right)^4 - \frac{[1 - (R_i/R_e)^2]^2}{2 \ln\left(\frac{R_e}{R_i}\right)}\right] \tag{6.21}$$

Finally, the average velocity will be found as:

$$\overline{w} = \frac{Q}{A} = \frac{Q}{\pi(R_e^2 - R_i^2)} = \left(-\frac{\Delta P}{\Delta z}\right) \frac{R_e^2}{8\mu} \left[1 + \left(\frac{R_i}{R_e}\right)^2 - \frac{1 - (R_i/R_e)^2}{2 \, ln\left(\frac{R_e}{R_i}\right)}\right] \tag{6.22}$$

6.1.3. MAXIMUM FLOW IN CONSTRICTED NOZZLE

In the previous paragraph we treated currents for incompressible fluids, thus we considered a constant density. Under this assumption and introducing a small perturbation in a volume of such a fluid, it is possible to demonstrate that the propagation velocity of the perturbation is infinite which means an instantaneous propagation. Nevertheless, if we now consider a compressible fluid, this velocity becomes finite. Moreover when the fluid is an ideal gas in a reversible (isoentropic) process, this velocity can be calculated as:

$$c = \sqrt{k \frac{p}{\rho}} = \sqrt{kRT} \tag{6.23}$$

Where p is the absolute pressure, ρ is the density, k is the ratio of the specific heats (≈1.4 for biatomic gases), R is the ideal gas constant and T is the temperature [K]

The speed c is the *sound velocity* since it is actually a good approximation for the velocity propagation of sound waves. Now we can define the so called *Mach number*, which express an adimensional ratio between the velocity of the gas and *c*.

$$M = \frac{v}{c} \qquad \begin{cases} M < 1 \text{ subsonic current} \\ M = 1 \text{ sonic current} \\ M > 1 \text{ supersonic current} \end{cases} \tag{6.24}$$

We will now consider the airflow through the nozzle in Figure 57. Air at the left of the nozzle is at rest pressure p_o and temperature T_o. The exit section is limited with *e*. The duct has a constriction in section *c*.

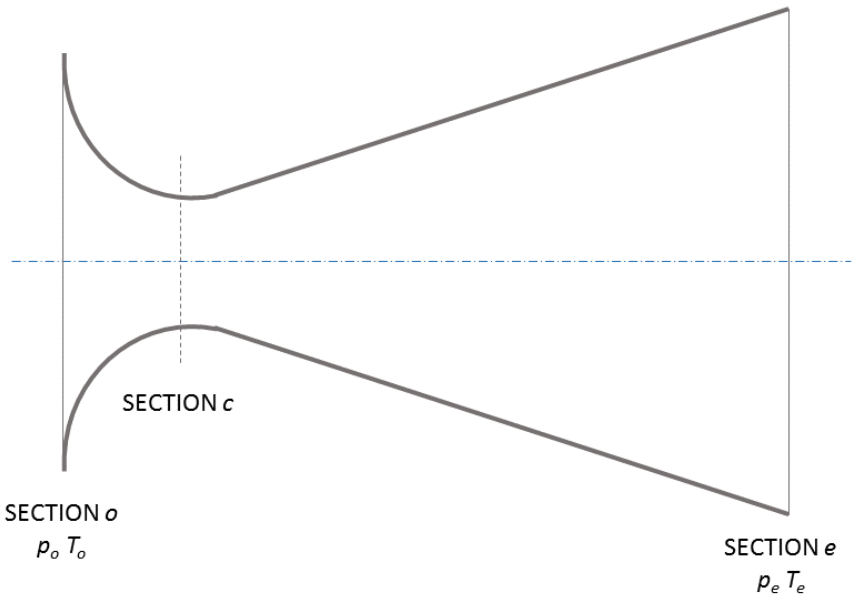

Figure 57 – Constricted nozzle

The fluid can reach sound velocity only when a local minimum of the duct section is present. In fact, when the flow is subsonic and the duct section decreases, there is acceleration of the fluid; so it is possible to reach the sound velocity. On the other hand, if the flow is supersonic a restriction causes a deceleration and, again, the sound velocity can be reached.

We will consider *M=1* in our section *c*: all the parameters and variables in this section will be named with a star *. It is possible to demonstrate that [26]:

$$\frac{T^*}{T_o} = \frac{2}{k+1} = 0.83333 \quad for \quad k = 1.4 \tag{6.25}$$

$$\frac{p^*}{p_o} = \left(\frac{2}{k+1}\right)^{\frac{k}{k-1}} = 0.52828 \quad \text{for} \quad k = 1.4 \tag{6.26}$$

$$\frac{\rho^*}{\rho_o} = \left(\frac{2}{k+1}\right)^{\frac{1}{k-1}} = 0.63394 \quad \text{for} \quad k = 1.4 \tag{6.27}$$

(6.25)-(6.27) are true only when *M=1* and for isoentropic processes. Therefore, the mass flow rate through the nozzle is:

$$\dot{m} = \rho u A = \rho^* u^* A^* = \rho^* c^* A^* = \rho_o \frac{\rho^*}{\rho_o} c_o \left(\frac{T^*}{T_o}\right)^{\frac{1}{2}} A^* \tag{6.28}$$

Where u is the average fluid velocity and A the duct section surface. Thanks to:

$$\rho_o = \frac{p_o}{RT_o}, \qquad c_o = \sqrt{kRT_o}, \qquad \rho_o c_o = p_o \sqrt{\frac{k}{RT_o}} \tag{6.29}$$

We can finally obtain:

$$\dot{m} = p_o A^* \sqrt{\frac{k}{RT_o}} \left(\frac{2}{k+1}\right)^{\frac{1}{k-1}+\frac{1}{2}} = p_o A^* \sqrt{\frac{k}{RT_o}} \left(\frac{2}{k+1}\right)^{\frac{k+1}{2k-2}} = 0.6847 \frac{p_o A^*}{\sqrt{RT_o}} \tag{6.30}$$

This means that the mass flow rate it is completely determined by the pressure and temperature in the input *section o* and by the area $A^*$of *section c*. Thus, even varying the pressure p_e, the flow rate will not be modified.

6.2. ITIA GRIPPER

We have completed the summary of the required fluid dynamics theory and so, now, it's time to apply these equations and formulae to our specific case, starting from the ITIA gripper. The following Figure 58 has the aim to show the main dimensions of the pneumatic circuit between the vacuum generator and the end-effector. In particular, the dimensions of the 4 mm duct were measured by us, while the ones of the 6 mm tube are taken from the Mitsubishi RP-1AH datasheet.

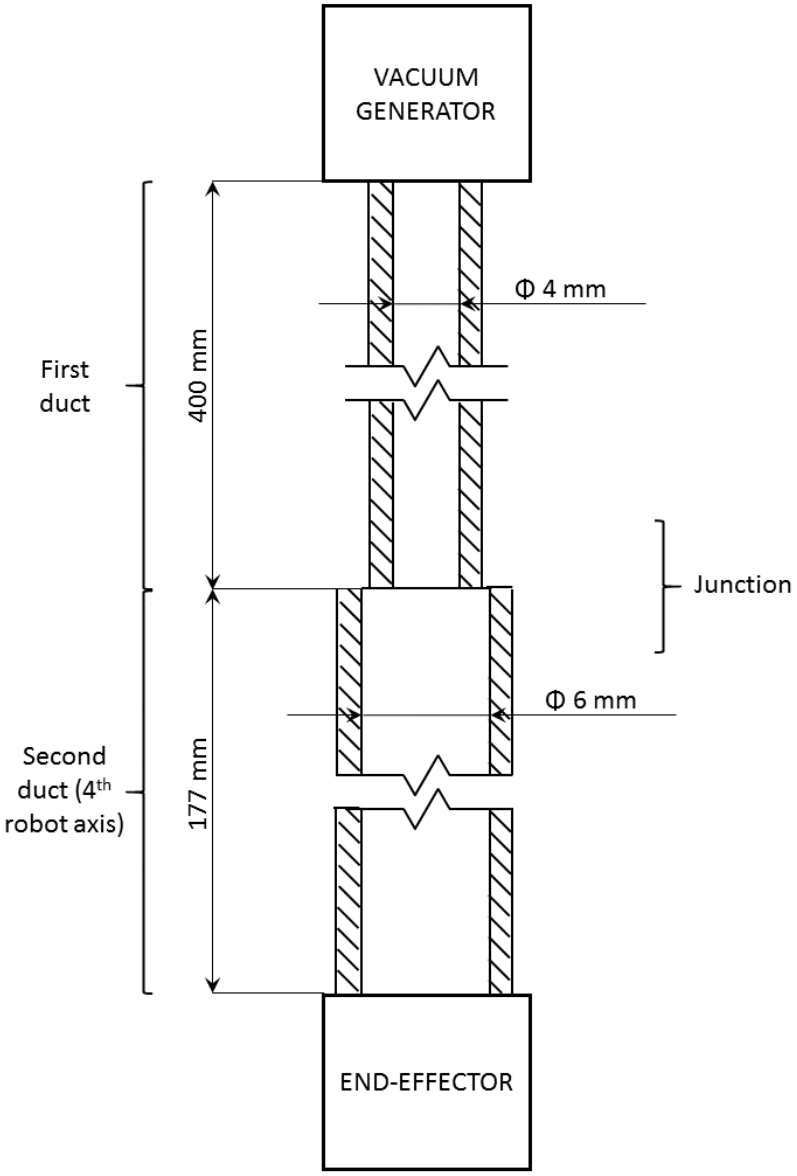

Figure 58 – Pneumatic circuit that actuates the ITIA gripper. It is composed by five main components: the vacuum generator, a tube with a diameter of 4 mm, the fourth axis of the robot with an internal diameter of 6 mm, a junction between those last two elements and finally the end effector.

We will now calculate the difference of pressure along the ducts, inside their junction and inside the gripper, using only the equations presented above, with no numerical simulation. We hope to find a plausible solution. We will treat air as a fluid with a dynamic viscosity of $1.98 \cdot 10^{-5}$ Pa·s in incompressible flow with density of 1.225 kg/m^3. We know also the vacuum degree of -70 kPa in correspondence of the vacuum generator (in this case the COAX© Micro Ti05-2) measured by a digital vacuum gauge; this value permits to find the volumetric flow rate of 0.02 nl/s from the datasheet (see chapter 4.3.2). The unit nl/s (normal litre per second) expresses the volume in

normal conditions: atmospheric pressures and 25°C. To convert this value in l/s we need to apply the ideal gas law:

$$PV = nRT \tag{6.31}$$

$$V = \frac{P_{atm}V_{normal}}{P_{operative}} \tag{6.32}$$

By doing this we find a flow rate of 0.065 l/s. Finally, the absolute difference of pressure is acquired as $P_{operative} = P_{atm} + VacDeg$, so 31.3 kPa. The value of vacuum degree found do not belong to the aspiration tests (chapter 5.2), but was registered with the ITIA gripper with the releasing mechanism mounted and an input pressure of 4 bar to the COAX© Micro.

6.2.1. DISTRIBUTED PRESSURE DROP

This difference of pressures is originated by the friction between the fluid and the wall. In addition to the velocity of fluid, they are also influenced by density and viscosity, by the diameter and the roughness of the wall. To calculate them we will use the Navier-Stokes exact solution applied to circular ducts. In particular, we will modify the equation (6.15) to express the difference of pressures as function of volumetric flow rate:

$$\Delta P = -\frac{8\mu Q \Delta z}{\pi R^4} \tag{6.33}$$

Then we will use equation (6.16) for the average velocity calculation.

These distributed pressure drops are located in our case in the ducts with diameters of 4 and 6 mm. The following table presents the numerical results.

	Pressure drop in the section [-kPa]	Average velocity of fluid [m/s]	Reynolds number
Tube of 4 mm	0.082	5.151	1275
Tube of 6 mm	0.007	2.289	850

6.2.2. CONCENTRATED PRESSURE DROP

On the other hand, additional pressure drops are associated the change of the cross-section area or a variation of the direction of the fluid. They are also located at the inlet or at the outlet of piping, in curves, elbows and so on. In our case, we must consider the junction between the tubes of 4 and 6 mm. Finding the exact difference of pressures is not an easy task but, since we are not expecting important pressure drops in this section, we will use an approximation. To study the worst possible case, we will suppose a brusque section change with the maximization of pressure drop [27].

$$\Delta P = \frac{1}{2} K \rho {V_m}^2 \tag{6.34}$$

Where V_m is the average velocity of fluid calculated as the mean between the velocities in the tubes already seen. K is a coefficient extracted from the Figure 59: the ratio between our sections is 0.66, so K is found upon linear interpolation between the inferior and superior values.

$$K = \frac{K_{sup} - K_{inf}}{r_{sup} - r_{inf}} \left(r - r_{inf}\right) + K_{inf} \tag{6.35}$$

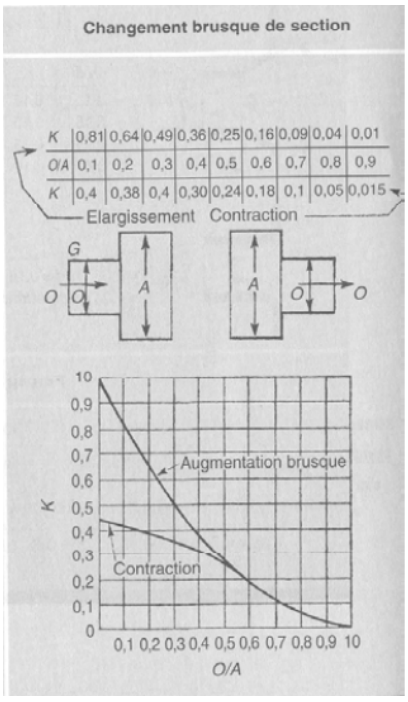

Figure 59 – Coefficient to calculate the concentrated pressure drop [27].

Even considering the worst case, the pressure drop calculated is only -0.001 kPa.

6.2.3. PRESSURE DROP INSIDE THE GRIPPER

Basing ourselves on the results of the previous paragraphs, we can conclude that:

- The flow in the ducts that connect the vacuum generator to the end-effector can be considered incompressible and laminar. Therefore the pressure drops can be estimated using the equation presented in paragraphs 6.1.1, 6.2.1 and 6.2.2.
- The total pressure drop is -0.09 kPa.
- The absolute pressure right above the gripper is: 31.21 kPa.

These data make us understand that the biggest difference of pressure is located inside the gripper. To calculate it we can try to apply the Navier-Stokes equations along the holed needle, treating that small tube as a ring-shaped duct. Therefore, knowing the geometry, we can apply the equations (6.21) and (6.22). Assuming that the internal release system is already lifted and is not moving, the data we are going to use are:

- R_i=0.075 mm, radius of the internal needle.
- R_e=0.13 mm, radius of the internal hole of the cannula.
- Δz=10.5 mm, length of the cannula.

$$\Delta P = -8\,\mu\,Q\,\frac{\Delta z}{\pi\,{R_e}^4}\,\frac{1}{\left[1-\left(\frac{R_i}{R_e}\right)^4-\frac{\left(1-\left(\frac{R_i}{R_e}\right)^2\right)^2}{2ln\left(\frac{R_e}{R_i}\right)}\right]} \tag{6.36}$$

$$\overline{w}=\frac{Q}{A}=\frac{Q}{\pi(R_e^2-R_i^2)}=\left(-\frac{\Delta P}{\Delta z}\right)\frac{R_e^2}{8\mu}\left[1+\left(\frac{R_i}{R_e}\right)^2-\frac{1-(R_i/R_e)^2}{2\,ln\left(\frac{R_e}{R_i}\right)}\right] \tag{6.22}$$

The results are unreasonable: ΔP=-247.6 kPa and $\overline{w}$=1827 m/s. The lack of consistency of those numbers made us understand that the simplifications done are too large: probably the smallness of diameters involved accelerate the fluid so much that the flow is no longer. In this case, we may have a situation similar to the one described in paragraph 6.1.3: therefore, even varying the

vacuum degree (by increasing the input pressure to vacuum generator), the mass flow rate will not change and the Poiseuille's solution cannot be applied.

6.3. RAPIDOGRAPH NIB

As already said, the largest difference between the dispenser gripper and the rapidograph nib is the presence of the lateral holes: we expect that the largest part of the flow rate passes through those elements and so, as a first analysis, we will not consider the small cannula. The fluid dynamics, in this case, may be treated as the flow were incompressible because the flow and section areas are much higher. In particular, we want to analyse the green pen with 6 bar as input pressure with the piINLINE Mini as vacuum generator. We will explain the method applied for the calculations in specific paragraphs, but we will report some preliminary numerical results in a different one to compare different levels of occlusion of lateral holes. The pneumatic circuit in this case is the same used for the aspiration tests (and it is sketched in Figure 60).

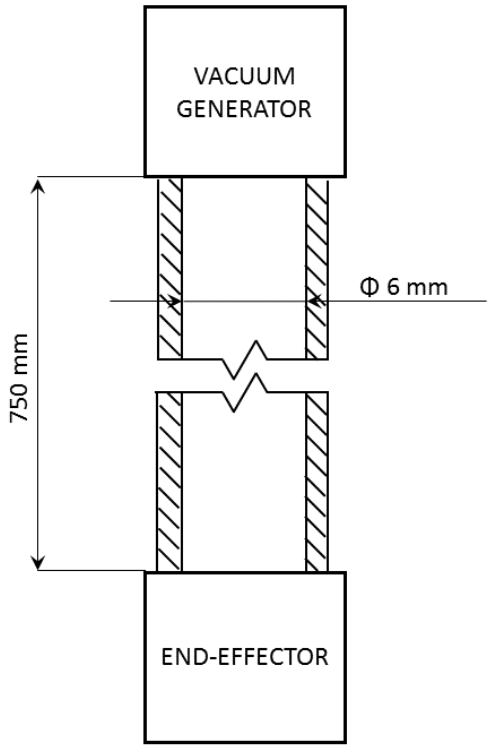

Figure 60 –Scheme of the pneumatic circuit used for the aspiration tests. It is composed by a vacuum generator that is connected to the end-effector through a 6 mm diameter tube.

6.3.1. DISTRIBUTED PRESSURE DROP

The calculation method is exactly the same seen before (paragraph 6.2.1) but the results will be much different. In this case, the vacuum generator let the passage of a larger airflow, increasing the pressure drops (as their linear correlation suggests). The equation used are (6.33) and (6.16) for difference of pressure and average velocity respectively.

6.3.2. FLUID DYNAMICS INSIDE THE GRIPPER

Even in this case we will use the same equation for the ring-shaped ducts but with different input data:

- R_i=1.3 mm, radius of the cylindrical weight upon the internal needle.
- R_e=1.7 mm, internal radius of the main chamber of the nib.
- Δz=22 mm, distance between the lateral holes and the gripper upper end.

We will apply equations (6.36) and (6.22) to find the pressure drop and the average velocity, but we will also calculate the Reynolds number (6.37) and the maximum theoretical liftable weight. For the former:

$$Re = \rho \frac{\overline{w} d S_{weight}}{\mu S_{weight}} = \frac{\dot{m}\, d}{\mu\, S_{weight}} \tag{6.37}$$

Where:

- $d = R_e - R_i$.
- $S_{weight} = \pi(R_e^2 - R_i^2)$.
- $\dot{m} = Q\rho$, where Q is measured in nm^3/s (normal cube metres per second), to be sure of the right value of ρ (not constant for compressible flow).

Finally, the maximum liftable mass depends on two effects: the difference of pressure caused by the vacuum and the drag generated by the airflow. For the first:

$$M_{max1} = -(\Delta P_{weight}\, S_2 + \Delta P_{needle}\, S_1) \frac{1}{g} \tag{6.38}$$

Where:

- ΔP_{weight}: is calculated with (6.36) and is the difference of pressure along the weight extension.
- $S_2 = \pi(R_i^2 - R_{needle}^2)$
- $S_1 = \pi\, R_{needle}^2$: is the cross-section area of the internal needle. For the green nib the R_{needle}=72.5 µm.
- ΔP_{needle} is the difference of pressure along the internal needle, supposing atmospheric pressure on one side and the vacuum degree (minus the pressure drop of the 6mm duct (6.36)) on the other.

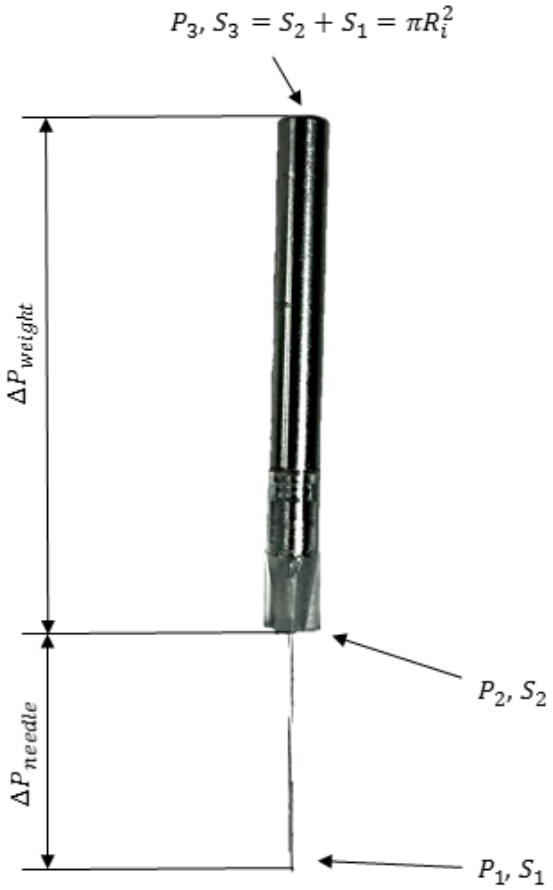

Figure 61 – Pressure scheme acting on the internal releasing mechanism.

The drag generated by a fluid on a wall is calculated with the *Newton formula* (6.39):

$$F(R_i) = \mu \frac{\partial w(R_i)}{\partial r} \tag{6.39}$$

$$M_{max2} = \frac{1}{g}\int_0^{2\pi}\int_0^{\Delta z} F(R_i)\, R_i\, d\vartheta dz = \frac{2\pi R_i\, \Delta z\, F(R_i)}{g} \tag{6.40}$$

We know that the distribution of velocity $w(r)$ (Poiseuille current) is a parabola with null values on the extremities (i.e. in correspondence of the walls due to the adherence boundary conditions). It is very easy to calculate the $\overline{w}$ with (6.22). Knowing the tendency of the function and its average value, we can determine its equation:

$$w(r) = K(r - R_i)(r - R_e) = K[r^2 - (R_e + R_i)r + R_e R_i] \tag{6.41}$$

$$\frac{\partial w(r)}{\partial r} = K(2r - R_e - R_i) \tag{6.42}$$

$$\frac{\partial w(R_i)}{\partial r} = K(R_i - R_e) \tag{6.43}$$

It is then possible to demonstrate that:

$$K = -\frac{6Q}{(R_e - R_i)^2 S_{weight}} \tag{6.44}$$

6.3.3. NUMERICAL RESULTS

The following table, as written before, contains the numerical results (calculated through some *MatLab* scripts) under different circumstances: when the lateral holes are fully opened, only one opened and in operative conditions. All the input data used are here reported (vacuum degree and flow rate) and were collected during the aspiration tests (chapter 5.2).

	Vacuum degree [-kPa]	Flow rate [nl/s]	Pressure drop in 6 mm tube [-kPa]	Pressure drop along the weight [-kPa]	Average veocity along the weight [m/s]	Reynolds number	M_{max1} [mg]	M_{max2} [mg]	M_{max} [mg]
Lateral holes fully opened	26	0.336	0.211	0.091	120	2205	93	652	745
One lateral hole opened	45	0.195	0.164	0.071	93	1280	114	506	620
Operative conditions	50	0.16	0.148	0.064	84	1050	118	456	574

Those calculus seem to be correct: in fact, remembering that the releasing mechanism for the rapidograph weighs 707 mg, the maximum masses $M_{max} = M_{max1} + M_{max2}$ found, are very closed to that value. As reasonable the contribute given by the drag greatly overcomes the other one. Of course, the information of the cases reported in the last two lines are in contrast with experimental evidences: in both cases the internal needle is lifted. However, comparing those numbers to the ones found in paragraph 6.2, we can conclude that, the model applied is not accurate but it estimate the correct order of magnitude. More importantly, those data give us useful information: Reynolds number indicates a laminar flow and the current is subsonic (M≈1/3). Thus, we are not under a chocked condition as in the ITIA gripper. Finally as soon as we introduce compressibility of the fluid in our model, the maximum theoretical liftable mass should increase. Those results practically represent an inferior limit and a very interesting starting point for future analysis (e.g. through numerical computation).

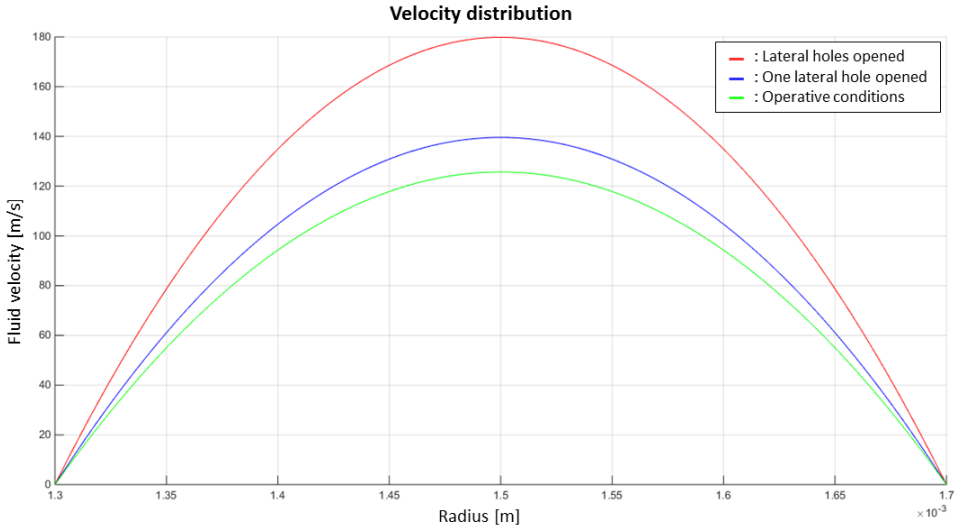

Figure 62 – Velocity distribution of the green rapidograph in the three analysed configurations.

7. CONCLUSIONS

Before the conclusion of this thesis, some considerations are necessary to summarise the results obtained. After the detailed descriptions made, we can expect that the ITIA gripper would lift heavier objects due to its larger inferior hole and consequently greater flow rate inside the cannula. On the contrary, the rapidograph's nibs may lift smaller parts but the release is guaranteed by the very heavy mass of inner needle. Since the larger the objects the heavier they are, we expect that if a component is lifted by ITIA gripper only, probably it weighs enough to fall with a very little help. On the contrary, smallest components that requires a heavier releasing system are very light and can be lifted by the technical pens.

Then, after the fluid dynamic model constructed, we can give a further explanation on why the internal releasing device of ITIA gripper, in some occasion, may be insufficient for the release: theoretically, when an object is grabbed it obstructs the cannula impeding the airflow. The object is solidly held due to the difference of pressure between the inside and outside of the gripper, but the internal mechanism falls because the pressure inside the end-effector becomes uniform and the flow rate is null (therefore both the conditions that raise the inner component disappear). Thus the internal needle lies touching the grabbed component. As soon as the vacuum pump is switched off, the difference of pressure quickly vanish and the grabbed object may either fall or

not. Its behaviour depends on the entities of adhesion forces that can overcome the weight tens of times (as seen in chapter 3). The ITIA gripper's internal component weighs about 5 mg, which is comparable to the component's mass and so it may not be enough to pledge the release. When we consider the functioning of the rapidograph's nibs, we have a quite different situation. In this case, we have two different airflows: one coming from lateral holes and the other coming from the small cannula. In this case grabbing the object closes the second flux only, while the first one (that is the largest) continues. This maintains the internal mechanism lifted, thanks to the high flow rate (chapter 6.3). Thus, the needle falls only when the vacuum generator is turned off: so the releasing is not only helped by the weight of the internal needle, but also from its linear momentum. The side effect is that such impulsive force can cause a severe decrement in performances, especially with object with non-flat surfaces (chapter 5.4.3).

7.1. FUTURE DEVELOPMENT

Several are the possible future development for this thesis: for instance, a new, more extended, set of pick and place tests should be carried out. Otherwise, another interesting idea would be lightening the internal release device of the rapidograph and measure again the accuracy and repeatability. After all, we can expect that even reducing the size of the internal mass, the 100% of releases should be guaranteed by the linear momentum during its fall. Nevertheless, such method may introduce some issues related to its excursion, that may require some kinds of adaptors.

Moreover, our analytic solutions can be a very interesting starting point for future fluid dynamics analysis through finite elements computation. Numerical resolution can give a more precise idea of the parameters involved like velocity distributions, pressures or walls' strains. We reported a very preliminary FEM study in the appendix of this work.

8. REFERENCES

[1] I. Fassi, G. Fontana, G. Legnani, C. Pagano and S. Ruggeri, “Dispositivo di manipolazione e metodo per manipolare a vuoto un componente”. Patent 0001416830, 26 March 2013.

[2] “Treccani - Enciclopedia,” [Online]. Available: http://www.treccani.it/enciclopedia/.

[3] “Hardware Upgrade,” [Online]. Available: http://www.hwupgrade.it/.

[4] “Intuitive Surgical - da Vinci Si Surgical System,” [Online]. Available: http://www.intuitivesurgical.com/products/davinci_surgical_system/davinci_surgical_system_si/.

[5] I. Fassi, *Slide of Microrobotics.*

[6] N. Chaillet and S. Régnier, *Microrobotics for Micromanipulation.*

[7] G. Fantoni, *Gripping Technologies.*

[8] "Wikipedia," [Online]. Available: https://en.wikipedia.org/wiki/Wikipedia.

[9] G. Raithel, *Electrostatic Morors.*

[10] C.-L. Di Jaime, W. E. Svendsen and M. Dimaki, Micro and Nano Techniques for the Handling of Biological Samples.

[11] S.-A. Zhou, "On fores in microelectromechanical systems".

[12] Festo, *Bernoulli grippers OGGB Datasheet.*

[13] CSEM, *Contactless Gripper with Ultrasonic Air Cushion.*

[14] Neild and Adrian, *Ultrasonic Contactless Gripper.*

[15] R. S. Fearing, "Survey of Sticking Effects for micro Parts Handling".

[16] E. Lifshitz, "The theory of molecular attractive forces between solids".

[17] H. D. Ackler, R. H. French and Y.-M. Chiang, "Comparisons of Hamaker Constants for Ceramic Systems with Intervening Vacuum or Water: From Force Laws and Physical Properties".

[18] Mitsubishi, *Datasheet Robot RP-1AH.*

[19] C. Umberti, *Slide del Corso di Impianti Idraulici.*

[20] "PIAB - Vacuum pump," [Online]. Available: https://www.piab.com/it-IT/Prodotti/pompe-a-vuoto/.

[21] PIAB, *Datahseet of COAX© Micro Ti05-2.*

[22] PIAB, *Datasheet of piINLINE© Mini Si 6-6.*

[23] W. Zesch, M. Brunner and A. Weber, “Vacuum Tool for Handling Microobjects with a Nanorobot”.

[24] G. Fonana, S. Ruggeri, C. Pagano, I. Fassi and G. Legnani, “Manipulation of microcomponents using vacuum grippers”.

[25] G. Fontana, S. Ruggeri, G. Legnani and I. Fassi, “Precision handling of electronic components for PCB rework”.

[26] D. Pnueli and C. Gutfinger, Meccanica dei fluidi.

[27] L. Puccinelli, *Corso di "Impianti e sistemi aerospaziali".*

[28] N. De Divitiis, *Corso di "Elementi di meccanica del volo".*

APPENDIX

In fluid dynamics, most of the times, the analytical solution of Navier-Stokes equations is not available due to their strong non-linearities. Rather, in most occasions, it is better to use a software for finite elements modelization. Such programs allow to find solutions even when the geometry is very complex or when the problem does not admit simplifications. To complete our work we tried to use numeric computation to gain some qualitative hints on of what happens inside our components. However the results we will present have to be considered just as preliminary and very gross.

ITIA GRIPPER

Unfortunately the theoretical approach tried in the chapter 6.2, didn't brought us to the hoped results. The complexity of the problem requires a detailed FEM analysis to complete the study of the gripper and to obtain quantitative results. We, therefore, used the software *Comsol Multiphysics* to accomplish this task. Thanks to the axis symmetry of the ITIA device, we could simplify the problem a lot, lightening the computational burden.

First of all, we proceeded making some simplification to the geometry as shown in Figure 63: the grey parts represent the air contained in the gripper and not the end-effector itself.

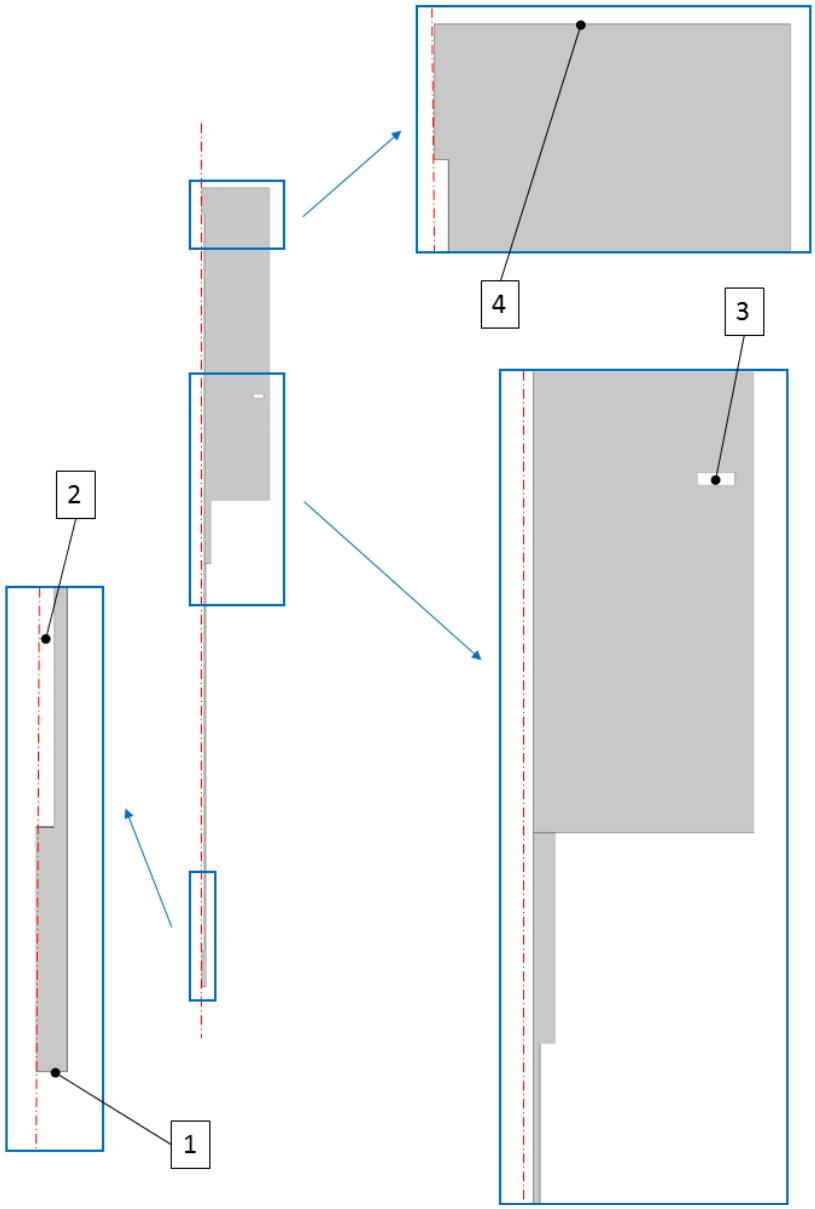

Figure 63 – The image represents the simplified model used for the numerical analysis. As the red axis suggests, the image contains just half model, the rest is obtained for symmetry. This scheme require an explanation: the grey parts represent the air contained inside the gripper, not the gripper itself. The parts 2 and 3 are the releasing mechanism (the needle and the disk respectively) longitudinally sectioned. Lines 1 and 4 are the projections of inlet and outlet surfaces.

As discovered in the chapter 6.2, a solver for compressible flows must be used. Beside we imposed the following boundary conditions:

- The atmospheric pressure as inlet condition (Figure 63 - label 1).

- The vacuum degree considering the distributed and concentrated pressure drops as outlet condition (Figure 63 - label 4).

We considered a laminar flow in stationary condition, the internal needle lifted and no object that obstructs the inferior hole. Under all those considerations we found the velocity distribution of fluid everywhere (Figure 64) and the pressures along the inferior and superior surfaces of the internal needle (Figure 65). We expect that the total pressure difference is distributed along the cannula only: for this reason we neglected the contribute given to the lifting force by the difference of pressure acting on the disk (Figure 63 - label 3).

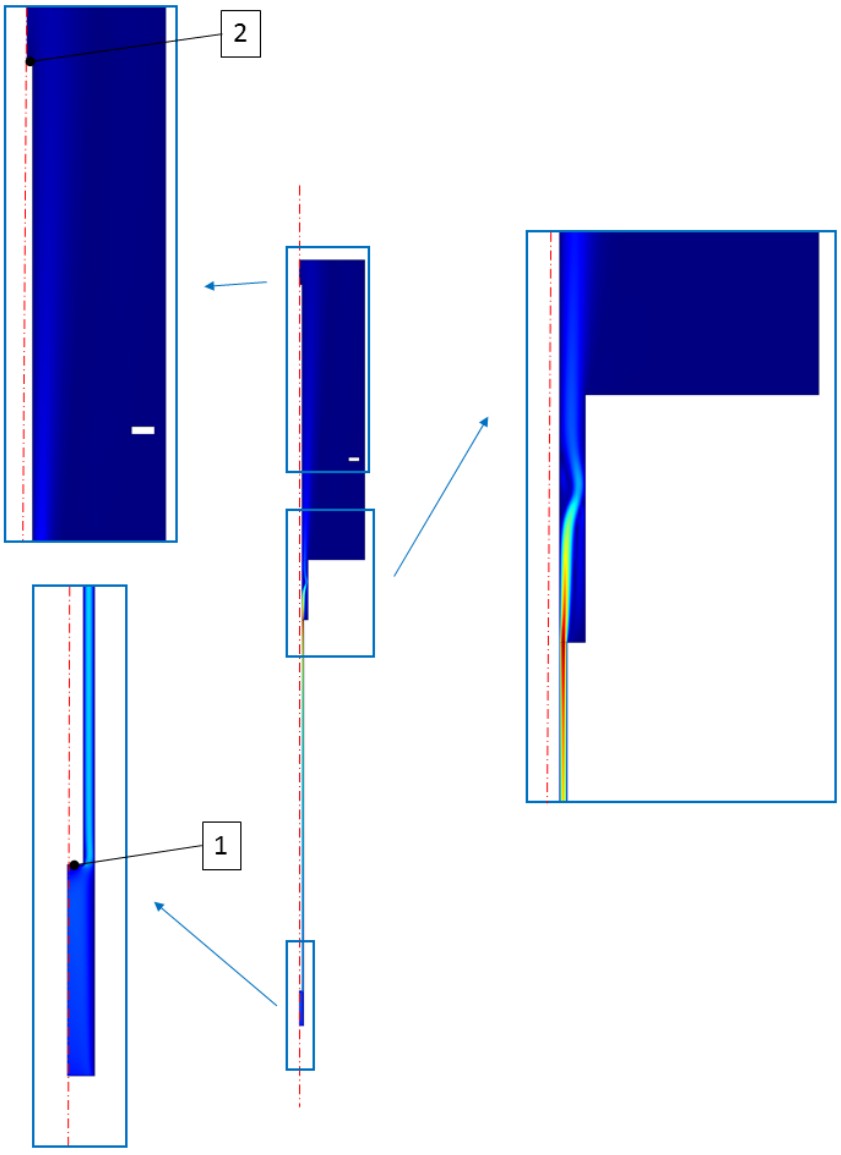

Figure 64 – The scheme shows the velocity distribution of the fluid inside the ITIA gripper. The colours corresponds directly to velocity values that have been exported to MatLab for further analysis. Finally along the lines 1 and 2 were calculated the pressures (Figure 65).

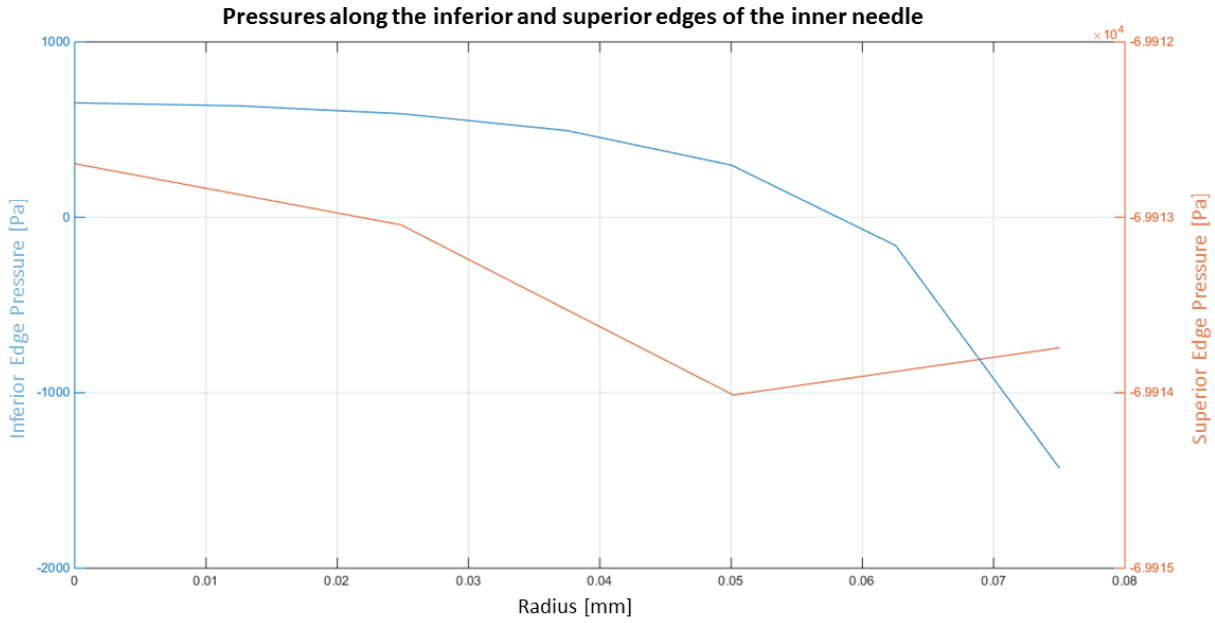

Figure 65 – Pressures along inferior and superior edges of the inner needle. In particular, the blue line represents the pressure curve along radius in the inferior surface (Figure 64 – label 1), the same for the red one but on the superior surface (Figure 64 – label 2).

All the data contained in figures Figure 64 and Figure 65 were exported to MatLab for further analysis. As explained in the previous chapter, the internal mass is lifted thanks to two actions: difference of pressure and drag. For the first one we calculated the average value of each curve in graph Figure 65 and so:

$$M_{max1} = \frac{1}{g}\left(\bar{P}_{sup} - \bar{P}_{inf}\right)S_{needle} \tag{7.1}$$

With $S_{needle} = \pi R_{needle}^2$. For the contribute given by the drag, instead, we exploited the formula to calculate the viscous friction force:

$$F_{friction} = \frac{1}{2}\rho C_d S_{lat}\overline{w}^2 \tag{7.2}$$

$$M_{max2} = \frac{F_{friction}}{g} \tag{7.3}$$

$$M_{max} = M_{max1} + M_{max2} \tag{7.4}$$

In the (7.2):

- $S_{lat} = 2\pi R_{needle} h$: is the lateral surface of the needle.

- $C_d = \frac{1.328}{\sqrt{Re}}$: is an aerodynamic coefficient calculated through the Reynolds number [28].
- $\overline{\omega}$: average velocity of the fluid, calculated as the mean of all the values represented in Figure 64.

Before reporting the numeric values, we must underline that this is just a brief FEM analysis and that the results are not necessarily correct. Thus, we would like to ask the reader to consider them qualitatively rather than quantitatively.

	Pressure on the upper part of the gripper [-kPa]	Difference of pressure along the needle [-kPa]	Average veocity of fluid [m/s]	Reynolds number	M_{max1} [mg]	M_{max2} [mg]	M_{max} [mg]
ITIA Gripper	69.9	70.14	12.2	56	126	16	142

The analysis confirms our suppositions: while for the rapidograph nibs the biggest contribution was given by the airflow drag, in this case the difference of pressure is much more important. In fact, we imagined that the flow rate is limited due to the constriction given by the narrowness of the needle. Another interesting consideration is that the output pressure exiting from the needle is inferior (in modulus) to the difference of pressure acting on the needle: the reason is that the flow enters the cannula and exerts a positive pressure on the internal needle in its inferior surface, thus the difference of pressure is increased.

RAPIDOGRAPH NIB

Even if we obtained interesting results with the theoretical approach, we decided to try a finite elements analysis also for the rapidograph nib. We used once again the green pen's dimensions to gain comparable outcomes and even in this case a simplification of the geometry was applied. The lateral holes are considered completely opened and the internal needle in lifted position. Unfortunately, the rapidographs are not axis symmetric due to their lateral holes: as a first attempt we decided to conduct a 3D modelization, but we could not find sound results. Therefore, we adopted again a 2D axis symmetric model (like for the ITIA gripper): for what concerns the lateral holes we decided to consider them as a single groove that practically cuts the rapidographs in two pieces. The Figure 66 should help to gain a better idea.

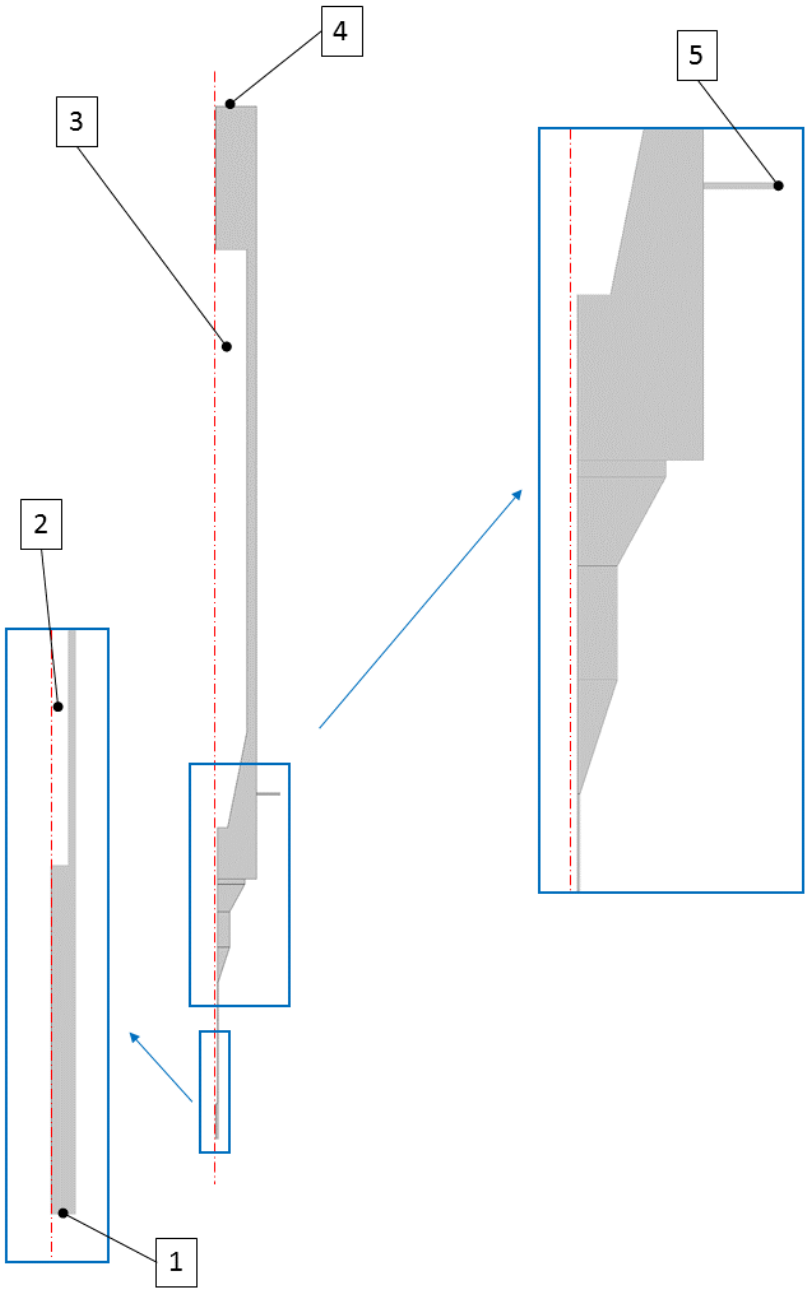

Figure 66 – Model of the green rapidograph used for the FEM analysis. As before, the grey parts are not the gripper itself rather the air inside; then the red axis expresses the symmetry of the component. The white parts 2 and 3 are the internal releasing mechanism (needle and weight respectively). Parts 1 and 5 are the inlet sections while the 4th is the outlet one. The small duct 5 consists in a groove that cuts the nib in two parts: its height has been determined imposing that the whole surface of this groove is equal to the surface of the two lateral holes.

The height of the small duct (Figure 66 - label 5) was found imposing the surface of the groove equal to the sum of the two lateral holes surfaces.

$$S_{groove} = S_{LatHoles} \tag{7.5}$$

$$2\pi R_{ext} h = 2\pi R_{LatHoles}^2$$

$$h = \frac{R_{LatHoles}^2}{R_{ext}}$$

Where $R_{LatHoles}$ is the radius of the each lateral hole and the R_{ext} is the radius of the rapidograph "main chamber". We can expect that this approximation is quite far from the reality for what concerns the neighbourhood of lateral holes, but it gets more and more accurate as soon as it comes closer to the outlet section. In fact, in the real device the air flux tends to become uniform, thus at a certain height the reality should be similar to the numerical solution.

As done before, in the next page we reported the Figure 68 with the velocity distribution inside all the gripper. It appears evident that the air flux comes totally from the lateral holes and nothing or a very small flow from the small cannula. Unfortunately, the study around the lateral holes is made even less precise by the coarseness of the mesh: in this small section, the software could not converge increasing the number of points.

However, the average velocity of the fluid along the ring-shaped duct around the weight is about 30 m/s. Since this value is almost a quarter than the one calculated before and considering all the limitations of this model, we decided not to keep any numerical results.

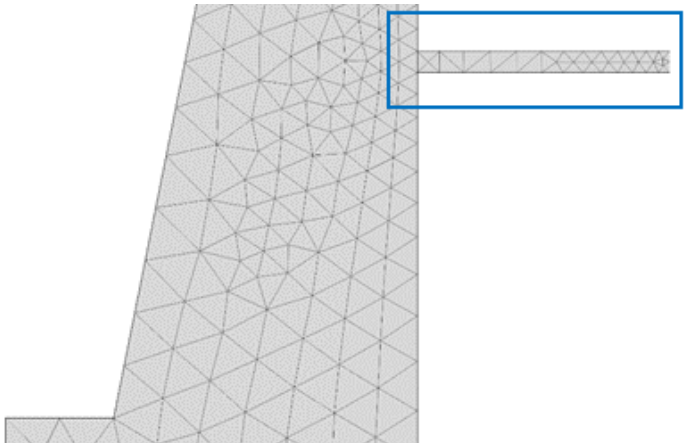

Figure 67 – Detail of the mesh coarseness along the small duct that simplify the lateral holes.

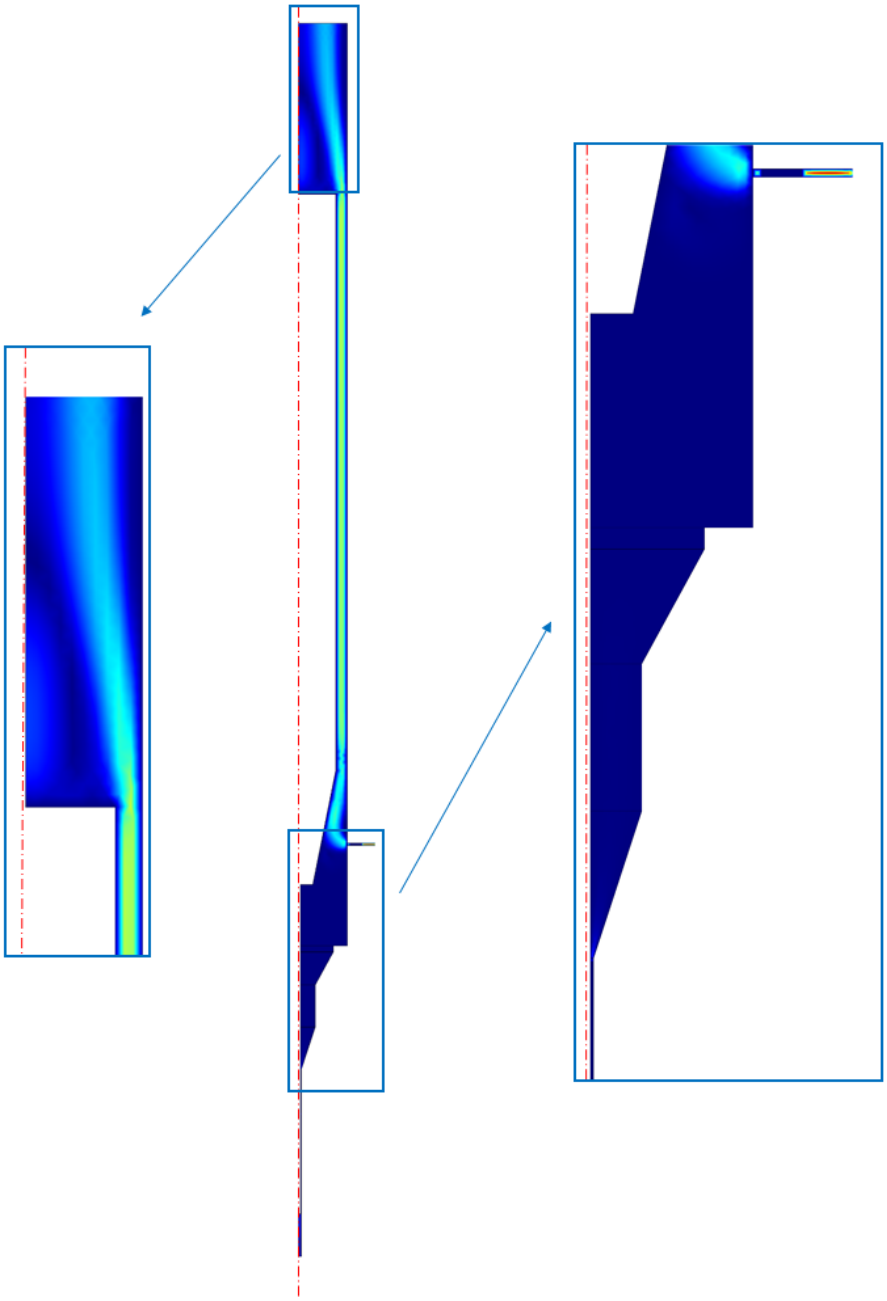

Figure 68 – Velocity distribution of the fluid inside the rapidograph nib. As reasonable, almost all the flow comes from the lateral holes and nothing from the small cannula.

ACKNOWLEDGEMENTS

Per concludere questo lavoro di tesi si rendono necessari alcuni ringraziamenti che scriverò in italiano essendo (per lo più) rivolti ad italiani.

Inizierei perciò ringraziando i miei relatori: i proff. Giovanni Legnani ed. Adriano Maria Lezzi che mi hanno seguito ed aiutato in ogni fase del lavoro e della stesura di questa tesi. A loro si sommano anche gli aiuti ricevuti dal personale di ITIA, ossia dalla prof.ssa Irene Fassi e dagli ingegneri Serena Ruggeri e Gianmauro Fontana, che mi hanno messo a disposizione in più occasioni il loro tempo ed il loro laboratorio. Sempre per quanto riguarda i docenti, desidero poi ringraziare anche i responsabili dei due progetti di doppio titolo di studio a cui ho partecipato. Ossia i proff. Manuel Berenguel Soria ed Antonio Visioli per quanto riguarda l'esperienza ad Almeria e le prof.sse Véronique Perdereau e Viviane Pasqui, oltre al già citato Giovanni Legnani, per il progetto di Parigi.

Il ringraziamento più grande è comunque rivolto a tutta la mia famiglia, in modo particolare a mia mamma, mio papà, mio fratello Marco e Dania. Il loro sostegno e la loro incrollabile pazienza (specialmente nel sopportare i miei frequenti sbalzi d'umore) mi hanno permesso di portare a termine brillantemente questo fantastico periodo della mia vita. Non solo, infatti il loro appoggio e la loro fiducia mi hanno sempre spronato a dare il meglio di me e migliorarmi costantemente in ogni aspetto della mia vita.

A questo punto rimangono da ringraziare gli amici, per i quali procederò a gruppi. Partirei dalla mia consona compagnia d'amici che riesce sempre a mantenermi allegro e di buon umore: non li elencherò per nome perché sarebbe lungo e correrei anche il rischio di dimenticarmene qualcuno. Passerò perciò ai compagni d'università ed in particolar modo agli *ingegneri di Parigi* (tra cui quel folle di Mattia): quante birre insieme e quanto COD! Un grazie speciale va poi al *club degli automatici* (Pasi, Tine e co.) ai quali non ho mai fatto mancare un certo carico d'ansia… sebbene controvoglia, tra loro devo citare Emanuele per avermi retto (e viceversa) per svariati mesi di convivenza forzata. Ultimi, ma non per importanza, ringrazio i ragazzi del *caffè letterario* cioè tutti i compagni del liceo (e anche qualcuno di più), che rivedo sempre volentieri e con cui condivido i meravigliosi ricordi di quegli anni. Tra questi, il più caro ricordo è certamente quello di Simone, grande amico che ricorderò per sempre per la sua grande simpatia.

Infine esprimo i miei più sinceri ringraziamenti a tutte le persone e gli amici che mi hanno sempre sostenuto e che non ho citato singolarmente solo per questioni di brevità.

UNIVERSITÀ DEGLI STUDI DI BRESCIA
UNIVERSIDAD DE ALMERÍA

Abstract

Often in microrobotics, the most critical moment while manipulating very small components is the releasing phase: some adhesion forces, that can be stronger than gravitational force, make this operation uncertain. As obvious, having an object that stays attached to the gripper during the releasing phase, it is a very unpleasant behaviour. The gripper studied in the course of this thesis, uses the vacuum as manipulation strategy, but tries to solve the issue of sticking forces adding a releasing mechanism. Aim of this work was to collect enough experimental data to realize a mathematical model of the end-effector, in order to highlight which parameters should be modified to increase performances (in terms of accuracy and repeatability).

Doble Título UNIBS-UAL

Mechatronics for Industrial Automation

Ingegneria dell'Automazione Industriale

Grado en Ingeniería Electrónica Industrial

Curso 2015/2016